

**GAIN MEASUREMENTS VIA SPONTANEOUS
EMISSION IN QUANTUM WELL SEMICONDUCTOR
LASERS**

**A THESIS
SUBMITTED TO THE DEPARTMENT OF PHYSICS
AND THE INSTITUTE OF ENGINEERING AND SCIENCE
OF BILKENT UNIVERSITY
IN PARTIAL FULFILLMENT OF THE REQUIREMENTS
FOR THE DEGREE OF
MASTER OF SCIENCE**

**By
Tolal Azfar
January 1996**

**TA
1700
A94
1996**

GAIN MEASUREMENTS VIA SPONTANEOUS
EMISSION IN QUANTUM WELL SEMICONDUCTOR
LASERS

A THESIS

SUBMITTED TO THE DEPARTMENT OF PHYSICS
AND THE INSTITUTE OF ENGINEERING AND SCIENCE
OF BILKENT UNIVERSITY
IN PARTIAL FULFILLMENT OF THE REQUIREMENTS
FOR THE DEGREE OF
MASTER OF SCIENCE

By

Talal Azfar

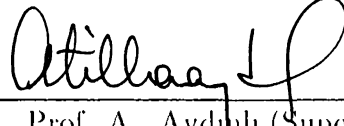
January 1996

Talal Azfar

TA
1700
-A34
1936

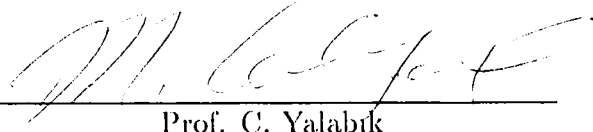
8033096

I certify that I have read this thesis and that in my opinion it is fully adequate, in scope and in quality, as a dissertation for the degree of Master of Science.



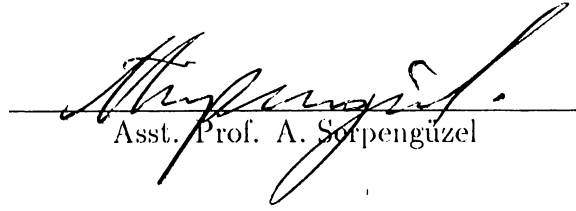
Prof. A . Aydin (Supervisor)

I certify that I have read this thesis and that in my opinion it is fully adequate, in scope and in quality, as a dissertation for the degree of Master of Science.



Prof. C. Yalabik

I certify that I have read this thesis and that in my opinion it is fully adequate, in scope and in quality, as a dissertation for the degree of Master of Science.



Asst. Prof. A. Sorpengüzel

Approved for the Institute of Engineering and Science:



Prof. Mehmet Baray,

Director of Institute of Engineering and Science

Abstract

GAIN MEASUREMENTS VIA SPONTANEOUS EMISSION IN QUANTUM WELL SEMICONDUCTOR LASERS

Talal Azfar

M. S. in Physics

Supervisor: Prof. A . Aydınli

January 1996

In this work an analysis of gain in single quantum well lasers as a function of some of their operational parameters is carried out. First, a theoretical model of gain is presented. Then two different methods of gain measurement, which use the spontaneous emission from the facet and the unamplified spontaneous emission from the top of the ridge, are discussed. Fabrication processes of lasers to facilitate the collection of unamplified spontaneous emission are detailed. Response of the gain spectrum to changes in injected current density and temperature are measured and understood in terms of band filling, band gap renormalization and temperature dependence of the bandgap. Gain saturation above threshold is verified and spatial variations in spontaneous emission in the longitudinal and lateral directions are observed.

Keywords: Quantum well, semiconductor laser, gain, spontaneous emission.

Özet

KUVANTUM KUYULU YARIİLETKEN LAZERLERDE KENDİLİĞİNDEN SALIM İLE KAZANÇ ÖLÇÜMLERİ

Talal Azfar

Fizik Yüksek Lisans

Tez Yöneticisi: Prof. A . Aydınlı

Ocak 1996

Bu çalışmada, tek kuvantum kuyulu lazerlerin kazanç özellikleri, bazı işletme değişkenlerinin işlevi olarak incelenmiştir. Önce, kütle ve kuvantum kuyulu yapılarda kazancın kuramsal modeli sunulmuştur. Sonra, kazancı belirlemek için, lazerin ön yüzünden toplanan kendiliğinden salım ile bu yüze dik yön de toplanan kendiliğinden salım metodları tartışılmıştır. Bu amaçla tasarlanan ve üretilen iki çeşit lazer yapısı ayrıntılı açıklanmıştır. Kazanç, eşik akım değerinin altında ve üstünde ölçülmüş ve kazanç doyumu gözlenmiştir. Kazanç spektrumunun sürülen akım yoğunluğuna ve sıcaklığa tepkisi ölçülmüş ve sonuçlar bant dolumu, yasak enerji aralığını renormalizasyonu ve sıcaklığa bağımlılığı ile açıklanmıştır. Düşük akım yoğunluklarında kovuk boyunca ölçülen kazanç değişiklikleri ayna kaybı ile açıklanmıştır. Son olarak ölçülen yatay kendiliğinden salım profili, yük taşıyıcılarının yatay yayılımını içeren bir model kullanılarak anlaşılmıştır.

Anahtar

sözcükler: kuvantum kuyu, yarıiletken lazerler, kazanç, kendiliğinden salım

Acknowledgement

It is my pleasure to express my utmost gratitude to my supervisor Prof. Atilla Aydınlı. I acknowledge his invaluable encouragement and appreciate his beneficial guidance throughout the development of my research work.

Here I wish to address my special thanks to Mr. Murat Güre for his sincere support in all stages of this work. I would also like to thank Mr. Güngör Singer for his help in the technical aspects of this research. I owe special thanks to Mr. İsmet İ. Kaya and Erhan P. Ata for their fruitful discussions and providing a stimulating research environment. I take this opportunity to thank Ms. Güşer Köseoğlu for her precious help during data acquisition.

Last but not least, I wish to acknowledge the vital moral support and motivation given by my friend Özgür Özer during the course of this project and in the moments of despair. I am debtful to him for providing a pleasant company, without which, life during the past year would have become unbearable.

Contents

Abstract	i
Özet	ii
Acknowledgement	iii
Contents	iv
List of Figures	vi
1 Introduction	1
2 Laser Fabrication	4
2.1 Quantum Well Structure :	4
2.2 GRINSCII Sample Structure :	5
2.3 Laser Fabrication Process	7
2.3.1 Metal alloy contact lasers	8
2.3.2 Indium Tin Oxide (ITO) contact lasers	14
3 Laser Diode Characterization	17
3.1 Basic spectral characteristics of Fabry-Perot cavity lasers	17
3.1.1 Fabry-Perot Resonator Modes	18
3.1.2 Resonator Modes and Threshold Gain	19
3.1.3 Mode Selection and Lasing	21
3.2 Optical Characterization of GRINSCII sample	25

3.2.1	Material Parameters	26
3.2.2	QW subband levels	27
3.2.3	Photoluminescence Study	29
3.3	Characterization of Laser Diodes	32
3.3.1	Current-Voltage Characteristics	33
3.3.2	Light Output vs Current Characteristics	34
4	Gain Measurements in Laser Diodes	38
4.1	Introduction	38
4.1.1	Methods of Measurement	39
4.2	Theoretical Model for Gain	39
4.3	Hakki-Paoli Method	50
4.3.1	Measurement Setup and Results	51
4.4	Gain Measurement using Unamplified Spontaneous Emission . . .	57
4.4.1	Relationship between Absorption and Emission	58
4.4.2	Gain vs. Injection Current	59
4.4.3	Effect of Temperature on Gain	63
4.4.4	Variation of Gain along the Cavity Length	64
4.4.5	Lateral variation in Spontaneous Emission Profile	67
5	Conclusions	71

List of Figures

2.1	Quantum Well Structure	5
2.2	GRINSCH Laser Material	6
2.3	Ridge Waveguide Laser Structure	7
2.4	Optical characteristics of Indium Tin Oxide	15
3.1	Fabry-Perot Resonator	18
3.2	Longitudinal Modes of Laser Cavity	21
3.3	Cavity Modes and Field Distribution in Laser.	22
3.4	Evolution of Lasing Mode	24
3.5	Subband Energy Levels of 3.9 nm Quantum Well	28
3.6	PL spectrum from ITO contact Laser	30
3.7	EL spectrum from ITO contact Laser at 0.6 mA current	31
3.8	I-V and I-P curves For an ITO contact ridge laser	32
3.9	Effect of heating on I-P curve of ITO contact lasers	34
3.10	Plot of $1/QDE$ vs. L of ITO lasers.	36
4.1	Calculated Gain in Bulk GaAs	47
4.2	Calculated Gain in GaAs Quantum Well	48
4.3	Broadening in QW gain spectrum	49
4.4	Spontaneous Emission Spectrum from Facet	51
4.5	Net Gain	52
4.6	Material Gain	56
4.7	Gain vs. Current	57
4.8	Unamplified Spontaneous Emission Spectra	59
4.9	Measured Gain in Laser	62

4.10 Unamplified Spontaneous Emission vs Temperature	63
4.11 Spontaneous Emission along Cavity Length at Very Low Injection	65
4.12 Spontaneous Emission along Cavity Length at 6 mA	66
4.13 Spontaneous Emission along Cavity Length above Threshold . . .	67
4.14 Lateral Profile of Spontaneous Emission Intensity	68
4.15 Spontaneous Emission from Off-Ridge Area	69

Chapter 1

Introduction

Quantum well lasers have evolved out of the traditional double heterostructure semiconductor devices. The double heterostructure (DH) lasers used thin semiconductor layers as the active region, typically on the order of a few hundred nanometers,¹ placed between two higher band gap materials. Due to the band gap discontinuity at the heterostructure boundaries a pinning of carriers under injection was made possible. This confinement resulted in a higher density of carriers in a relatively smaller region compared to the earlier P-N junction based devices and helped lower the threshold currents of the lasers.² A need for even better localization of carriers and the technological developments enabling the fabrication of high quality, ultra thin semiconductor layers by methods such as Molecular Beam Epitaxy (MBE) paved the way to the realization of quasi two dimensional structures in semiconductors. The quantum well structure provided a control over the emission wavelength of the lasers by adjusting the thickness of the well layer and offered reduced density of states in the conduction and valence bands, compared to the bulk semiconductors.³ The gain of quantum well structure is about an order of magnitude greater than bulk system.⁴ This high gain helped in fabricating lasers with even lower threshold current densities and improved the quality of semiconductor lasers. The first observation of quantum well laser operation was made by J. P. van der Ziel et al⁵ in 1975. Tsang,⁶ with an introduction of graded index waveguide, has shown that lasers with threshold

current densities as low as 160 A/cm^2 and internal quantum efficiencies of up to 95 % can be manufactured.

An important parameter in semiconductor laser diodes is the gain. Its behavior, both below and above lasing threshold, as well as its spectral behavior is critical in understanding the characteristics of the laser diodes and design of new laser diode structure. However, due to the difficulty of measurement of gain spectra of an operating laser diode, as testified by P. Rees,⁷ relatively few measurements of gain are reported in the literature. Several different measurement methods have been used in this respect. Both the spectral dependence of gain as well as its dependence on the injected carrier density have been reported for a limited number of materials and laser structure. From these data spectral broadening due to interband scattering, resulting in a smoothing of the gain spectra expected from sharp density of states, is also documented.

In this work, we intended to design and fabricate Graded Index Separate Confinement Heterostructure (GRIN SCH) Single Quantum Well (SQW) semiconductor laser diodes and study the behavior of gain as a function of various operational parameters, such as injected carrier density, temperature, etc. In our study we used two different approaches to measure gain, the Hakki-Paoli method and the unamplified spontaneous emission (USE) method. Both of these methods have been preferred by several workers over other measurement techniques. Hakki-Paoli method uses the facet emission of a laser to determine the gain spectra. The USE method depends on the measurement of spontaneous emission from laser in a direction perpendicular to the quantum well plane. This type of spontaneous emission does not face any amplification in the active region of the laser and is therefore termed as the unamplified emission. Commonly, the collection of this emission is made by making an opening in the n-type ohmic contact of the laser but in this way the spontaneous emission usually experiences absorption in the substrate. Kesler et al⁸ have fabricated lasers with a narrow opening in the p-type contact of the laser, over the ridge of the laser, and measured the spontaneous emission through this opening.

We have fabricated both the window-in-the-contact type lasers and the

transparent ohmic contact lasers, which allows us the collection of unamplified spontaneous emission of the laser through both the p-type and the n-type ohmic contacts. In the second chapter the description of the laser sample structure is given and the fabrication process of both of these lasers are explained. Third chapter contains the results of some fundamental characterization of the laser sample material and laser diodes as they pertain to the gain. Thus, electrical and optical characteristics of these lasers are investigated and their results are discussed. Fourth chapter deals with the gain measurements in semiconductor lasers. First, a theoretical model of gain is presented and the phenomena of gain in semiconductor lasers is analyzed. This is followed by a brief description of each of the two measurement techniques. The experimental results obtained by these methods are then presented and briefly discussed. Evolution of gain in response to the injected carrier density is analyzed and effects of temperature and spatial variations are discussed. Finally, a brief conclusion of the work is presented in the fifth chapter.

Chapter 2

Laser Fabrication

2.1 Quantum Well Structure :

When a very thin layer (on the order of a few tens of nm), e.g. of GaAs, is sandwiched between two higher band gap semiconductor materials, e.g. $\text{Al}_x\text{Ga}_{1-x}\text{As}$, we obtain the quantum well (QW) structure. A carrier trapped in this layer experiences a confinement in the sense similar to the classical problem of a particle in a box. This confinement leads to the development of a set of discrete energy levels in conduction and valence bands of the QW layer as shown in Fig.2.1. The position of these levels are a function of the thickness of the well layer as well as band offsets, thus enabling control over the wavelength of the emitted photons due to recombination of carriers. Even more remarkable feature of the quantum wells is the staircase density of states profile in these bands, resulting in a reduced density of states compared to the 3D bulk materials used as active region in the DH lasers. This characteristic of quantum wells then makes the population inversion in the active region easier.⁴

In addition to the carrier confinement in the quantum well, the surrounding layers, due to their lower refractive index, also provide a natural wave guide for photons generated in the QW layer. The quality of the waveguide and optical mode confinement can be improved by engineering the surrounding layers accordingly, as is the case in the graded index layers of waveguide in the

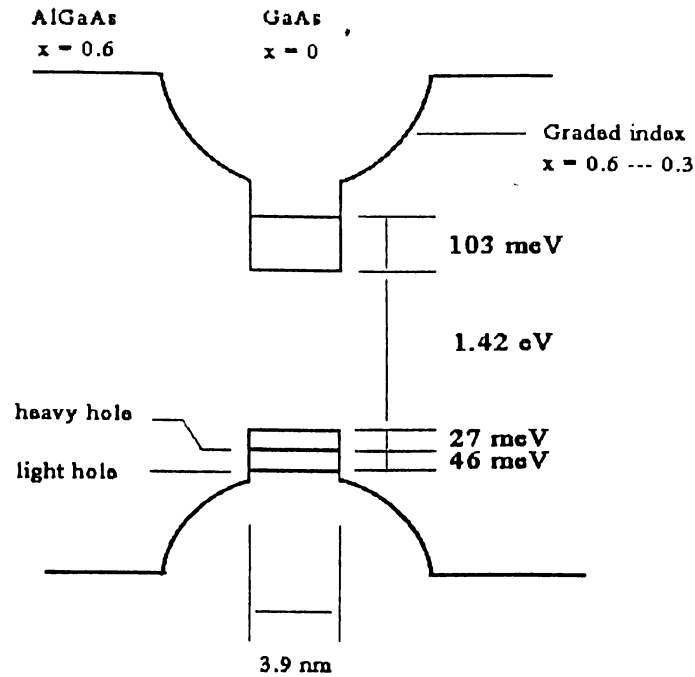


Figure 2.1: Quantum Well Structure

Quantum well structure formed by a 3.9 nm GaAs layer sandwiched between two $\text{Al}_{0.3}\text{Ga}_{0.7}\text{As}$ waveguide layers. The waveguide AlGaAs layers are graded.

GRINSCH lasers.⁴ These features of the quantum well structure have further reduced the threshold currents of semiconductor lasers.

2.2 GRINSCH Sample Structure :

The samples used to fabricate lasers in our experiment were MBE grown GRINSCH single quantum well wafers, commercially acquired from EMF International, Inc.

Starting from the substrate these samples consisted of the following layers: First, over a n-type doped GaAs(001) substrate, a $0.5 \mu\text{m}$ thick n^+ -type GaAs buffer layer has been grown to increase the surface quality and to obtain defect free surfaces for further growth. Later, a $1 \mu\text{m}$ thick n-type $\text{Al}_x\text{Ga}_{1-x}\text{As}$ ($x=0.15$)

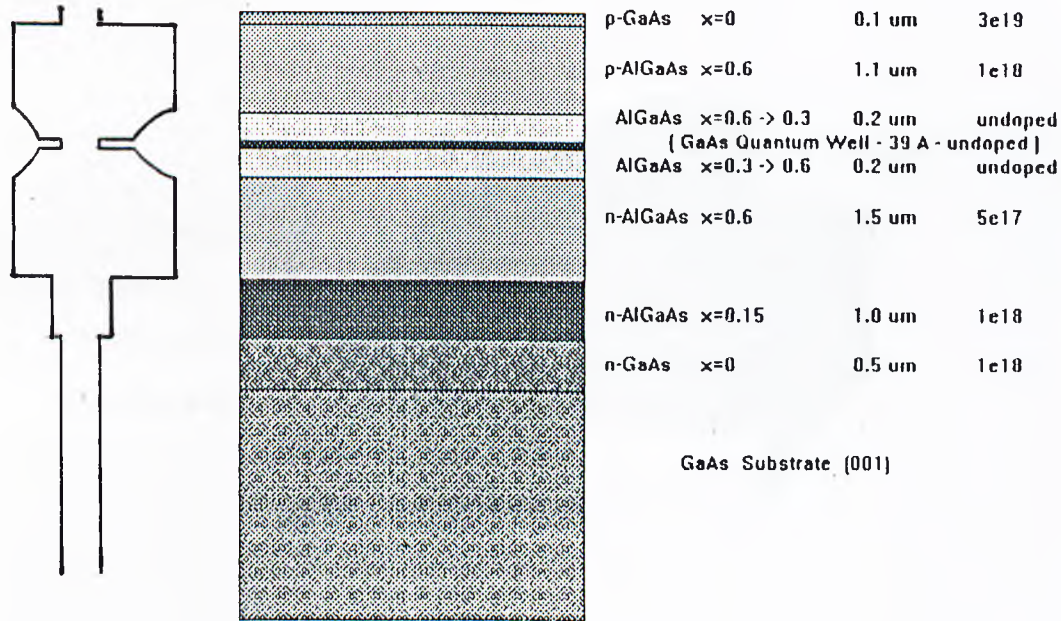


Figure 2.2: GRINSCH Laser Material

The composition and structure of GRINSCH laser sample used to fabricate lasers. A band diagram of the GRINSCH sample is also shown.

intermediate layer has been grown. This is followed by the first, so called, cladding layer of 1.5 μm thick $\text{Al}_x\text{Ga}_{1-x}\text{As}$ ($x=0.6$) and then the two 0.2 μm thick waveguide layers of $\text{Al}_x\text{Ga}_{1-x}\text{As}$ having a 3.9 nm thick undoped GaAs quantum well active region, sandwiched between them. The undoped wave guide layers are graded with a parabolic profile having their Al concentration decreasing from 0.6 to 0.3 at the quantum well edge. Following the upper wave guide layer, the p-type region starts with the second cladding layer of 1.1 μm thick p-type doped $\text{Al}_x\text{Ga}_{1-x}\text{As}$ ($x = 0.6$). Finally, to obtain a good ohmic contact, a 0.1 μm thick highly p-type doped GaAs layer has been grown. The doping density of various layers and the energy band lineup of the sample is shown in Fig. 2.2.

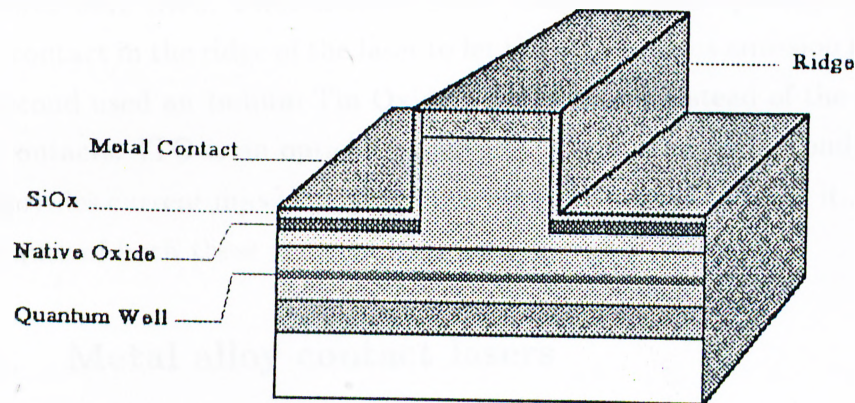


Figure 2.3: Ridge Waveguide Laser Structure

2.3 Laser Fabrication Process

The most commonly used laser structure is the ridge waveguide structure, shown in Fig.2.3. This structure utilizes a ridge mesa on the p-doped side to define the path of injected current. The ohmic contact on the p-side of the sample has a thin layer of oxide everywhere underneath it, except over the ridge of the laser. This oxide layer prevents injection of carriers through any other part of the upper contact except the ridge itself. Though relatively more difficult to fabricate, an injection of carriers through only a narrow window of the whole contact, made possible by the ridge mesa structure, decreases the loss of current in the sample and increases the carrier density in the active layer during injection, making it preferable over structures such as broad contact lasers. This increased density of carriers by injection through mesa in turn helps lower the threshold current of the laser.

To enable collection of spontaneous emission from the laser in a direction perpendicular to the quantum well plane, fabrication of two different types of structures were tried. First of these used a narrow stripe opening in the p-type metal contact in the ridge of the laser to let the spontaneous emission be collected. The second used an Indium Tin Oxide (ITO) contact instead of the usual metal alloy contacts. ITO is an optically transparent and electrically conductive oxide and provides current injection while allowing light to pass through it. Fabrication techniques of both these types of lasers are discussed below.

2.3.1 Metal alloy contact lasers

The process steps for the fabrication of our metal alloy contact ridge waveguide lasers are summarized as follows;

Wafer cutting

The sample wafer come in a 2 inch diameter circular form with about half a millimeter in thickness. The surface of these samples are oriented along the (100) plane and the primary flat along the ridge of the wafer defines the (011) plane. The (011) family of planes defines a natural cleavage direction for GaAs. Small square pieces of about 1 cm are then cut from these wafers keeping the sides parallel to the (011) set of planes for easier cleaving and high mirror quality.

Sample cleaning

The samples were first subjected to a multi-step sequential rinsing treatment by various chemicals to free them of any dirt or residual oxide layers. They were immersed in hot TriCholoroEthane(TCE), hot acetone and propanol solution at room temperature, in the described order, for two minutes each. It is vital to apply this sequence without letting the sample get dry between any two chemical treatments. The samples were then dried under continuous Nitrogen gas flow after being thoroughly washed by deionized water. The cleaning procedure was repeated until a completely clean sample surface was obtained.

Photolithography

Photolithography is used to define the ridge pattern on a sample by using photo-resist, and a mask. This process starts with a deposition of a thin uniform layer of photo-resist over the sample which is then covered with the mask and exposed to ultraviolet light. The areas of the photo-resist not covered by the mask patterns are thus exposed to this light forcing them to go under chemical changes. For a positive photo-resist the exposed areas are then removed by dipping the sample in a developing solution, leaving the mask pattern copied on to the sample defined by the residual unexposed photo-resist.

To define the ridge of the laser the photolithography was performed using a positive photo-resist. A $1.1\ \mu\text{m}$ thick homogeneous film of AZ-5211E photo-resist over the sample was obtained by spinning the sample at 5000rpm for 30 seconds. Prior to the deposition of photo-resist, 100% HexaMethylDisilazene (HMDS) solution was spun on the sample to increase the adhesion of the resist. The samples were then soft-baked in oven at $90\ ^\circ\text{C}$ for 40 minutes. Mask alignment and exposition steps were carried out by following conventional photolithography techniques with Karl-Suss MJB-3 Mask Aligner. Samples were exposed under $12\ \text{mW}$ -UV light for about 38 seconds. A quartz mask containing $1.4\ \text{cm}$ long stripes of various widths, ranging from $1\ \mu\text{m}$ to $50\ \mu\text{m}$, was used to define the ridge pattern. After exposure the samples were dipped in Toluene for 10 minutes for easier lift-off process. Developing was done using AZ-400K Developer diluted in the deionized (DI) water. Finally the samples were carefully rinsed in DI water and dried using dry nitrogen.

Reactive ion etching

The mesa were etched using Reactive Ion Etching (RIE) process, commonly known as dry etching. This step was performed in Leybold-LE 301 parallel plate (planar) reactive ion etching system using Cl_2 gas. The process was performed using the following parameters :

Gas flow rate = $8.0\ \text{sccm}$

Gas pressure = 7.0×10^{-3} mbar

Inverse of gas conditioning factor ($1/GCF$) = 1.18

Gas conditioning time = 64 sec

RF power = 13 W

Capacitor voltages: $C_s = 129$ Volts, $C_p = 325$ Volts

The etch rate obtained using this recipe was around 500 nm/minute. This rate is much higher than the traditionally used CCl_2F_2 gas etch rates. As the required mesa depth was over 1 μm a high etch rate was desirable. Chlorine, though, is a very reactive gas and we observed a thin dark film left over the etched areas of the sample after the dry etching by chlorine. An XPS analysis of this film revealed presence of Ga, As and Al oxide along with traces of fluorine. This film was very stable and was very difficult to remove using HF or HCl acid. As these etched areas were going to be covered with an oxide layer later on and current was not going to be injected through these areas, the presence of this film did not hamper the performance of our lasers.

Native oxide growth

Following the RIE of the sample, a 0.1 μm thick layer of native oxide was grown using the standard anodic oxidation technique. The term Native Oxide is defined as the surface oxide product that is formed when the surface of GaAs host crystal is consumed in an oxidizing ambient. The anodic oxide solution is prepared by first mixing Ethylene Glycol: Citric acid: DI water with a ratio of 200ml : 3gr : 97ml, followed by an addition of Ammonia solution till the pH level of the whole solution reaches 6.5. The oxide grown using this solution contains a mixture of various oxides of Ga and As and possibly the hydrates thereof. Native oxide growth consumes some of the sample and it was observed that for every 10 nm of oxide layer formed, 4 nm of the sample was consumed and replaced by the oxide, while the remaining 6 nm of the oxide resides over it. Beside forming a barrier to current, this oxide layer helps passivating the surface defects, formed during the dry etch of the sample.

PECVD of silicon dioxide

To further improve the quality of oxide current barrier layer, a $0.1\mu\text{m}$ thick dielectric layer of SiO_x over the native oxide was grown using the Plasma Enhanced Chemical Vapor Deposition method. PECVD at low temperature deposits a uniform good quality oxide film which is free of surface defects. This oxide layer smoothens the inhomogeneities in the native oxide layer. The process parameters were as follows :

APC pressure = 300 mTorr

RF power = 10 W

LP strike = 2000 mTorr

Temperature = 100°C

Gas Flow Rates : $\text{SiH}_4 = 180 \text{ sccm}$, $\text{N}_2\text{O} = 710 \text{ sccm}$

The deposition rate was approximately 15 nm/minute and a smooth and homogeneous film of SiO_x was obtained.

Lift-off process

After the deposition of SiO_x layer the photo-resist layer over the ridge, and along with it the SiO_x layer on top of it, was removed by lift-off leaving the ridge area free of any oxide and ready for the metallization of ohmic contacts. In the lift off process the resist is dissolved in acetone and it breaks away with it any material on top of it.

Window stripe pattern

To open a small stripe-window over the ridge, in order to obtain spontaneous emission, a second photolithography step was repeated in much the same way as the earlier step but with a narrower stripe than the width of the ridge. The window-stripe was centered in the ridge using the alignment markers on the mask.

Metallization of p-type ohmic contact

P-type metallization included evaporation of 30 nm of Ti immediately followed by an evaporation of 120 nm of Au on the surface of the sample. Leybold L560 Box Coater was used for the evaporation of these materials and a chamber pressure on the order of 10^{-6} mbar was achieved before the process was initiated.

Second lift-off process

The window in the metal covered ridge was opened using the lift-off technique and by removing the photo-resist stripe pattern obtained during the second lithography. The metal covering this window-stripe was also removed in the lift-off leaving a bare GaAs surface.

Annealing

To obtain the ohmic contacts following the p-type metallization, samples were thermally treated at 430 °C in a Rapid Thermal Annealer oven for one minute. Annealing forms an alloy of the contact metals and also helps in the reduction of the series resistance of the sample.

Thinning

To facilitate an easier dicing of the lasers the overall thickness of the sample was reduced to 100 μm by chemically thinning the substrate at the back side of the wafer. A solution of $\text{H}_2\text{O}_2 : \text{NH}_3$, in a ratio of 10:1, was used for wet etching. The top side of the samples were protected by sticking the top surface of the sample to a thin glass plate using the photo-resist and heating it for about 40 minutes in the oven at 90 °C. No penetration of the etching solution to the top side was observed during the thinning process. After the thinning the samples were separated from the glass by acetone.

Metallization of n-type contact

Much like the metallization of p-type contact, n-type contacts were made by evaporating Ni/Au/Ge/Au layers, in the described order, on the back side of the samples. The thickness of various layers were 35:60:25:125 nm respectively.

Annealing

The n-type ohmic contact quality was improved by annealing the samples at 460 °C for about one minute.

Dicing and separation

The samples were then diced by cleaving the samples in a direction perpendicular to the ridge stripes to form good quality mirrors for the lasers. The lasers were then separated from each other resulting in a typical laser dimensions of $500\mu\text{m}$ by $500\mu\text{m}$ a piece.

Discussion

Several problems arose during the fabrication of these type of lasers. First of all, the alignment of window stripe over a thin stripe of ridge caused some problems. For example when the dimensions of the ridges were reduced to $1\mu\text{m}$, a $2\mu\text{m}$ opening left only $1\mu\text{m}$ of metal contacts on each side of the window, thus reducing the contact area and forcing us to increase the ridge width to window width ratio. Even more severe problem arose during the second liftoff. As the window stripes were quite narrow acetone could not penetrate through these stripes effectively, resulting in a poor lift off, leaving pieces of metal on top of these openings. The second lift-off became nearly impossible with gold layer thickness increasing above 150 nm.

This forced us to decrease the thickness of the gold layer but it resulted in thinner deposition of the metals on the side walls of mesa structure. These thin metal contact layers on the side walls can breakdown under high bias conditions. To avoid this problem side walls of the mesa were covered with metal more

efficiently by tilting the samples sideways during the metal deposition but this in turn caused an already difficult liftoff process to become even more challenging. These problems forced us to have compromise on the ridge and the window widths of these lasers.

After trying several different combinations of ridge and window widths we finally succeeded in fabricating a laser with $50\mu m$ ridge having a $7\mu m$ opening on top of it. These lasers were tested and were seen to lase with a threshold current of about $65mA$, and spontaneous emission from the top of the ridge could be collected. These lasers had high threshold currents due to a large ridge width. The equipment available for pulse biasing the lasers in the laboratory was not able to provide such high currents effectively without considerable noise. An attempt to DC bias these lasers resulted in an acute heating of these lasers and the samples were badly damaged. The lasers are usually cooled under DC biasing by first mounting their top side on a continuously cooled surface. The requirement to collect the spontaneous emission from the window on the top contact prevented us from mounting them from their top side. The lasers were tried to be cooled through the substrate side but at higher currents the heating became inevitable.

These problems forced us to look for a radical solution and a solution was found by incorporating a ITO layer for p-type contact.

2.3.2 Indium Tin Oxide (ITO) contact lasers

Indium Tin oxide can be used to make both the p-type and the n-type ohmic contact to GaAs. Usually used in the vertical emitting surface lasers, this oxide is transparent in the wavelength range of the emitted light in our GRINSCII structure, with a transmittance reaching up to 80 percent or more (Fig. 2.4). Annealing of ITO improves both the ohmic and the optical properties of the contact.

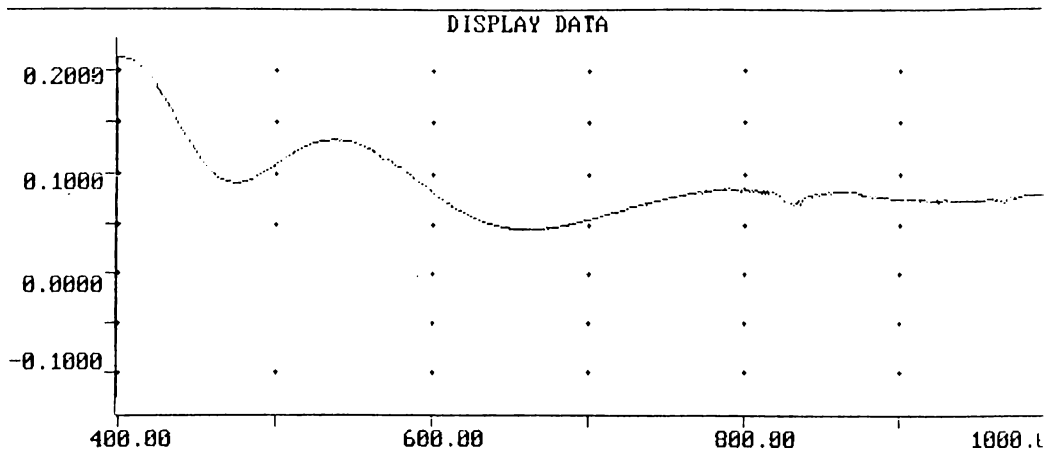


Figure 2.4: Optical characteristics of Indium Tin Oxide
Absorbance spectrum of ITO thin film sputtered on glass

Process optimization

These properties of ITO were ideal to solve our problem and we decided to replace the top metallic contact by the ITO contact. During the initial optimization of this process ITO was sputtered over bare GaAs and oxide covered GaAs test samples to investigate the contact properties of ITO. Soon it was discovered that though the ITO makes a good ohmic contact to bare GaAs, if ITO is deposited over the SiO_2 layer and annealed at above $360\text{ }^\circ\text{C}$, bubbles start to form on the contact surface and it peels off from the sample. The contact quality degrades drastically as the annealing temperature goes above $400\text{ }^\circ\text{C}$. It was also seen that if SiO_2 layer is not used and ITO is directly deposited over the native oxide layer the Annealing temperature needs to be further reduced, down to $300\text{ }^\circ\text{C}$, for a stable contact. This forced reduction in Annealing temperature meant

that the usual n-type metal alloy contact, requiring an annealing temperature above $400\text{ }^{\circ}\text{C}$ for a good ohmic contact, needed to be modified as well. This did not pose a very serious concern as ITO can be used for n-type contact as well, though the contact quality was not going to be as good as the metal alloy contact. In addition it was also possible to trade off between depositing SiO_2 over the native oxide layer but having to lift it off later on and not depositing SiO_2 at all, as a $0.2\mu\text{m}$ thick layer of native oxide was seen to be sufficient to stop any current injection by itself, and getting rid of the difficult lift off process entirely. Although not depositing the SiO_2 meant annealing temperature needed to be reduced to $300\text{ }^{\circ}\text{C}$, the lack of lift off process made a very thin ridge laser fabrication feasible. Therefore it was decided to remove the deposition of SiO_2 from the process and make a $4\mu\text{m}$ wide ridge waveguide single mode laser.

Fabrication process

Fabrication process for the Indium Tin Oxide contact laser is similar to but much simpler than the window-opening metal alloy contact lasers. The samples are separated and cleaned as before. The ridges are defined by photolithography and mesa are formed by dry etching, much like in the previous case. Instead of $0.1\mu\text{m}$, a $0.2\mu\text{m}$ thick layer of native oxide is grown gradually to form a homogeneous layer. The photoresist over the ridge is then removed by acetone and ITO is sputtered over the sample to form the p-type contact. Samples are annealed at $300\text{ }^{\circ}\text{C}$ for one minute and then thinned down to $100\mu\text{m}$. To form the n-type contact again ITO is used and sputtered over the substrate side of the laser followed by a second annealing at $300\text{ }^{\circ}\text{C}$. The samples are then diced to separate individual lasers of desired cavity lengths. For our experiments we fabricated a $4\mu\text{m}$ wide ridge laser.

Chapter 3

Laser Diode Characterization

3.1 Basic spectral characteristics of Fabry-Perot cavity lasers

The photons generated in the active region of the QW semiconductor laser can experience a negative absorption (i.e. amplification) if the population inversion condition in the medium is satisfied. By confining these photons in a resonator and ensuring a feedback in the cavity a self-stimulating oscillation (i.e. laser action) can be produced. The properties of the beam emitted by a QW laser depend on the shape and dimensions of the resonator and on its position with respect to the active region.⁹

The optical feedback in our laser diodes is effected by means of the Fabry Perot resonator. The resonator is created by closing the dielectric waveguide at its ends by two plane mirrors formed by the two smooth cleaved surfaces of the crystal which are perpendicular to the quantum well plane. The surfaces of the remaining two side walls of the crystal are rough as to avoid unwanted radiation modes.

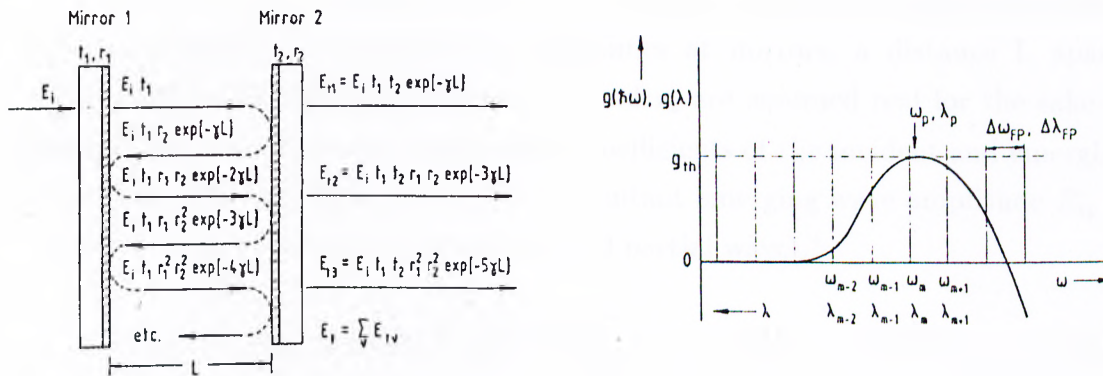


Figure 3.1: Fabry-Perot Resonator

An example of the superposition of linearly polarized wave in a Fabry-perot resonator and the resonance frequencies vs. spectral distribution of gain in a cavity. Taken from [4]

3.1.1 Fabry-Perot Resonator Modes

The behavior of light generated in the active layer can be approximated as plane waves travelling in a rectangular waveguide for an index guided laser.¹⁰ Moreover, these plane waves have been shown to be dominantly linearly polarized in a direction parallel to the QW plane in lasers. In index guided structures, the waveguiding is achieved by setting the active zone in a strip waveguide. Besides the buried hetrostructure lasers, suitably constructed ridge waveguide lasers can also behave like index guided lasers. Therefore we can gain an understanding of the lasing behavior in our semiconductor laser by an analysis of the linearly polarized plane waves in Fabry-Perot cavity.

Figure.3.1 shows schematically the propagation of plane waves in a Fabry-Perot resonator. The propagation constant of the monochromatic wave $\gamma = \alpha/2 + i\beta$ is complex, where α is the absorption coefficient and β is the wavenumber. An incident wave, polarized in the y direction, with the complex amplitude E_{iy} is reflected back and forth many times at mirrors, a distance L apart. The amplitude reflection coefficients r_1 and r_2 are assumed real for the sake of simplicity. The amplitude transmission coefficients of the incident and emerging waves are denoted by t_1 and t_2 . The resultant emerging wave amplitude E_{ty} is found by superposition of the transmitted partial waves.⁴

$$E_{ty} = t_1 t_2 E_{iy} \exp\{-\gamma L\} \sum_{\nu=0}^{\infty} [(r_1 r_2)^\nu \exp\{-2\nu\gamma L\}] \quad (3.1)$$

which can be reduced to

$$E_{ty} = E_{iy} \frac{t_1 t_2 \exp\{-\gamma L\}}{1 - r_1 r_2 \exp\{-2\gamma L\}} \quad (3.2)$$

since γ is complex, the amplitude of the transmitted wave is a periodic function of the wavenumber $\beta = 2\pi n/\lambda$.

3.1.2 Resonator Modes and Threshold Gain

If the denominator in the equation 3.2 becomes zero, an incident wave of finite amplitude produces a transmitted wave of infinitely large amplitude. This is the condition for self stimulation (i.e. laser oscillation)

$$r_1 r_2 \exp\{-2\gamma L\} = 1 \quad (3.3)$$

This is also known as the threshold condition. The relation between the propagation constant γ , the absorption coefficient α and the refractive index n is⁴

$$\gamma = \frac{2\pi i}{\lambda} \left(n - i \frac{\alpha \lambda}{4\pi} \right) \quad (3.4)$$

The absorption coefficient α is the sum of the gain g of the laser transition and the intrinsic losses of the cavity α_i

$$\alpha = \alpha_i - g \quad (3.5)$$

and then the equation 3.3 can be rewritten as

$$r_1 r_2 \exp\{(g - \alpha_i)L\} \exp\left\{\frac{4\pi n L}{\lambda}\right\} = 1 \quad (3.6)$$

The amplitude therefore gives the threshold condition

$$r_1 r_2 \exp\{(g - \alpha_i)L\} = 1 \quad (3.7)$$

and the phase gives the resonance condition of the cavity

$$\frac{4\pi n L}{\lambda} = 2m\pi \quad (3.8)$$

which determines the possible eigenwaves or modes of the system. Here m takes the positive integer values and determines the number of half wavelengths that are present in the cavity at a given λ . This condition indicates the wavelengths at which any laser emission is to be expected. The separation between two neighboring modes $\Delta\lambda_{FP} = \lambda_m - \lambda_{m-1}$ is found to be

$$\Delta\lambda_{FP} = \frac{\lambda^2}{2Ln(1 - (\frac{\lambda}{n})(\frac{dn}{d\lambda}))} \quad (3.9)$$

For example the cavity modes of our ridge laser with a cavity length of 520 μm are shown in Fig.3.2

With negligible dispersion in the active medium, i.e. $\frac{dn}{d\lambda} = 0$, the corresponding angular frequency separation is

$$\Delta\omega_{FP} = \frac{\pi c}{Ln} \quad (3.10)$$

The frequency separation is independent of the frequency and depends only upon the intrinsic characteristics of the cavity.

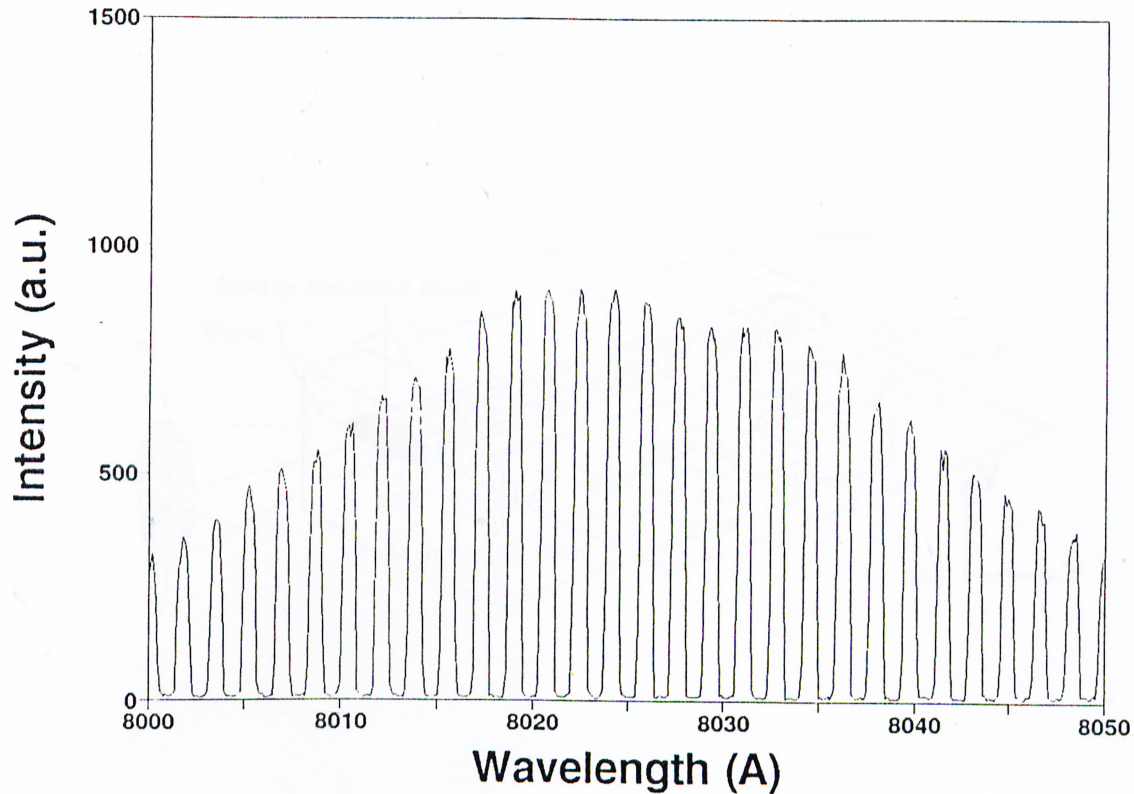


Figure 3.2: Longitudinal Modes of Laser Cavity
Longitudinal resonance modes of an ITO laser with a 520 μm long cavity.

3.1.3 Mode Selection and Lasing

In reality the active region of the laser in our Fabry-Perot cavity laser makes a rectangular three dimensional waveguide for the light. In addition to the cleaved mirror surfaces of laser, called the facets, cavity behavior in the other two orthogonal directions is formed due to the difference of the refractive index of the active region and its surroundings.¹¹ In the direction parallel to the QW plane, the GaAs layer is sandwiched between lower refractive index AlGaAs layers. Also the current injection changes the refractive index of the active area compared to regions where the carrier density is lower. Accordingly, we may distinguish the three types of modes : longitudinal modes which are formed between the facets of the laser along the length of the cavity, transverse modes and lateral modes, along x and y axes, respectively. Fig.3.3. The modal spacing of all three types of mode

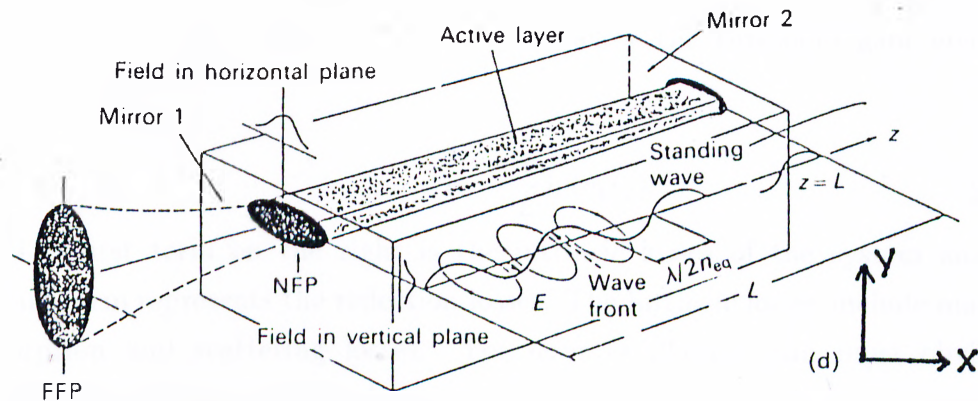


Figure 3.3: Cavity Modes and Field Distribution in Laser. Far Field Pattern (FFP) and Near Field Pattern (NFP) of a Fabry-Perot cavity laser are shown. Field distributions in the lateral (x -axis) and transverse (y -axis) direction are also given. Taken from [31]

can be determined by equation 3.10, where L represents the distance between the facets of the laser for longitudinal modes, width of the active region for lateral modes and the thickness of the active layer for transverse modes. While the spectral behavior of the laser is determined by the longitudinal modes its spatial distribution and characteristics are governed by the lateral and transverse modes.

The selection of the lasing wavelength is done from the longitudinal modes of the cavity by the gain profile of the active medium. The width of the gain curve is usually much larger than the mode separation of the cavity and many modes are encapsulated by the overall gain profile. If amplification is caused by current injection one can assume as a first approximation a linear relationship between peak gain g_p and injected carrier density n^+

$$g_p = a(n - n_t) \quad (3.11)$$

where a is the differential gain $\frac{dg_p}{dn}$ and n_t is the transparency density of the carriers. The gain always remains at or below the threshold gain given by equation⁹

$$g_{th} = \alpha_i - \frac{1}{L} \ln(r_1 r_2) \quad (3.12)$$

The first term on the right is the intrinsic losses of the system and the second term represents the reflection losses. The intrinsic losses include material absorption and scattering losses. For laser oscillation gain must obviously compensate for the intrinsic losses and the reflection losses. Laser oscillation will occur at wavelengths which satisfy the resonance condition of the cavity and at which the amplification is at the same time great enough to outweigh the losses.

This phenomena for our ITO contact laser with a ridge width of $4 \mu m$ and a cavity length of about $520 \mu m$ is shown in Fig.3.1. At 12 mA current we see a nearly flat curve with oscillatory modes having a nearly equal intensity. As the current is gradually increased and threshold current of the laser is approached a few modes develop out of this scheme. Finally at 16 mA current one of the mode wins over and the laser starts to lase in a predominantly single mode at wavelength around 802.4 nm. The intensity of this modes is far greater than other modes and at this stage it is practically a single mode laser. The single mode behavior is one of the most important difference of the index guided lasers from gain guided lasers, which have nearly always a multi mode behavior.

The selection of transversal modes in the resonator of a junction laser chiefly results from the fact that for a given m -th order mode and a given waveguide structure, i.e. given n_1 and n_2 , the refractive indices of AlGaAs and GaAs respectively for our case, the thickness d of the active layer has a critical value d_m defined by^{9,4}

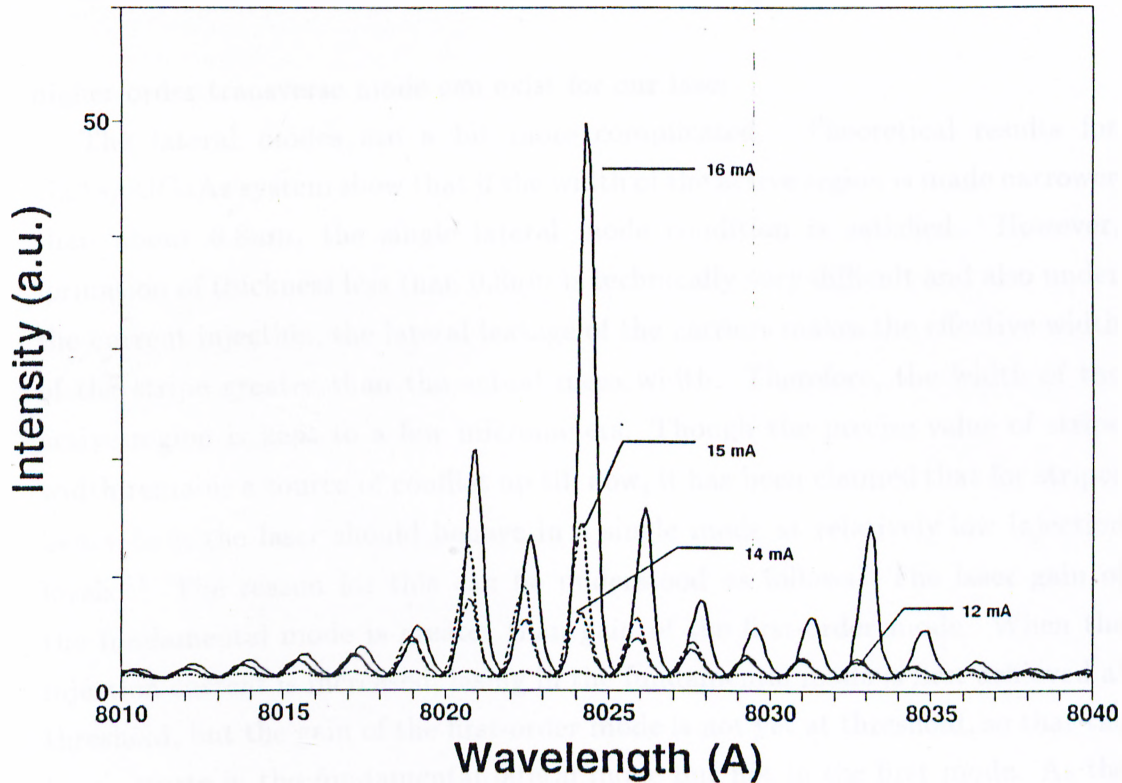


Figure 3.4: Evolution of Lasing Mode

Lasing mode selection in the ITO contact laser with an increase in Injection current. The threshold current of the Laser is 16 mA

$$d_m = m \frac{\lambda}{2} (n_2^2 - n_1^2)^{-1/2} \quad (3.13)$$

where $m = 0, 1, 2, 3, \dots$ and $m = 0$ is the fundamental transverse mode. If the thickness d of the active layer becomes smaller than d_m , the m -th order mode is no longer confined within the central layer. As a result, its electromagnetic field spreads out into the cladding layers almost freely, leading to an abrupt increase of the diffraction losses so that the threshold condition cannot be fulfilled and the mode cannot be excited. It should be noted that the fundamental mode is always excited. For our laser the refractive index of central GaAs active layer is 3.590 and that of surrounding $Al_{0.3}Ga_{0.7}As$ is 3.385 which leads to a critical thickness of about $0.3 \mu m$ for the first mode. As our quantum well layer is just 3.9 nm thick it clearly satisfies only the fundamental mode condition and no

higher order transverse mode can exist for our laser.

The lateral modes are a bit more complicated. Theoretical results for GaAs/AlGaAs system show that if the width of the active region is made narrower than about $0.8\mu\text{m}$, the single lateral mode condition is satisfied. However, formation of thickness less than $0.8\mu\text{m}$ is technically very difficult and also under the current injection, the lateral leakage of the carriers makes the effective width of the stripe greater than the actual mesa width. Therefore, the width of the active region is kept to a few micrometers. Though the precise value of stripe width remains a source of conflict up till now, it has been claimed that for stripes below $5\mu\text{m}$ the laser should behave in a single mode at relatively low injection levels.¹¹ The reason for this can be understood as follows. The laser gain of the fundamental mode is greater than gain of the first-order mode. When the injection current is increased, lasing in the fundamental mode is first achieved at threshold, but the gain of the first-order mode is not yet at threshold, so that the lasing starts in the fundamental lateral mode but not in the first mode. As the injection current is further increased, the gain of the fundamental lateral mode reaches saturation, while the gain of the first-order mode continues to increase and reaches threshold. Then the first order mode starts lasing at a much higher injection current.⁹

This phenomena though is not very simple and beside the development of higher order lateral modes spatial variations in the near field pattern have been observed with an increase in the current.^{11,2} Complications might also arise due to the inhomogeneities in the mirror surfaces and imperfections in the cavity.¹¹

3.2 Optical Characterization of GRINSCH sample

Photoluminescence (PL) study of a sample is a good technique to characterize the material and reveals the optical characteristics of the sample. In order to analyze the emission properties of the quantum well and of other layers in the

sample, if any, a photoluminescence (PL) study of the GRINSCM laser sample was carried out. This analysis helps in understanding the energy band structure of the quantum well.

In the first part of this study a theoretical calculation of various possible energy levels of the quantum well under consideration was done. This calculation later helps in understanding the complex features of PL spectra and to locate the signal position from the quantum level and to differentiate it from the signals generated in any other layers.

3.2.1 Material Parameters

The thin layer of GaAs, a few nanometer thick, placed between AlGaAs layers constitutes a quantum well heterojunction structure. The band gap of $\text{Al}_x\text{Ga}_{1-x}\text{As}$ is a function of Al concentration, given as⁴;

$$E_g = 1.424 + 1.274x \quad (3.14)$$

Al concentration also affects the refractive index of $\text{Al}_x\text{Ga}_{1-x}\text{As}$ according to the relation⁴;

$$n_r = 3.590 - 0.710x + 0.091x^2 \quad (3.15)$$

The higher bandgap of the $\text{Al}_x\text{Ga}_{1-x}\text{As}$ creates a potential well for the carriers in the GaAs conduction and valence bands. The carriers trapped in this potential well experience a confinement in the direction perpendicular to the plane of the quantum well layer only, creating discrete energy levels in the conduction and the valence bands which can be denoted as E_{cn} and E_{vn} respectively. The subscript n , takes integer values as 1,2,3,..., denoting different energy subbands in the well. Assuming a parabolic energy band profile for the carriers in bulk material, the total energy of electrons and holes in conduction and valence bands of quantum well layer, parallel to y - z plane, can be given as⁴

$$E_{cn}(k) = E_{cn} + \hbar^2/2m_e(k_y^2 + k_z^2) \quad (3.16)$$

$$E_{vn}(k) = E_{vn} - \hbar^2/2m_h(k_y^2 + k_z^2) \quad (3.17)$$

where m_e and m_h are the effective masses of electrons and holes in the conduction and valence bands, respectively. The wave vector k has a fixed x -component : $k = (k_{xn}, k_y, k_z)$. The energy at the n th subband edge is $E_{cn} = \hbar^2/2m_e(k_{xn}^2)$ for conduction band and $E_{vn} = \hbar^2/2m_h(k_{xn}^2)$ for the valence band. The wave vector components k_y and k_z can take arbitrary values.

The two-dimensional character of carrier motion is then apparent if the thickness of the quantum well is smaller than the scattering length of the free charge carriers and also smaller than the de-Broglie wavelength of the particles based on their thermal excitation.⁴ In GaAs, the scattering length of electrons at room temperature is about 50 nm, and the de-Broglie wavelength for electrons and holes at thermal excitation $\Delta E = kT$ is

$$\lambda_{e,h} = 2\pi\sqrt{\hbar^2/(2m_{e,h}\Delta E)} \quad (3.18)$$

which is about 30 nm for electrons and about 10 nm for holes. As our sample contains a quantum well of 3.9 nm, it clearly satisfies the above criterion.

3.2.2 QW subband levels

A simple estimate of the energy subband levels in the quantum wells can be made using a particle in a finite well model. Consider the GaAs-AlGaAs potential well system, Fig.3.5. Letting the potential difference between GaAs and AlGaAs as the height of the potential well, U_0 , and the energy of the particle in the well as E , we obtain the well known set of equations¹²

$$\beta a = \alpha a \tan(\alpha a) \quad (3.19)$$

$$\beta a = -\alpha a \cot(\alpha a) \quad (3.20)$$

where a is half the well width and

$$\alpha = \sqrt{2m^*E/\hbar^2} \quad (3.21)$$

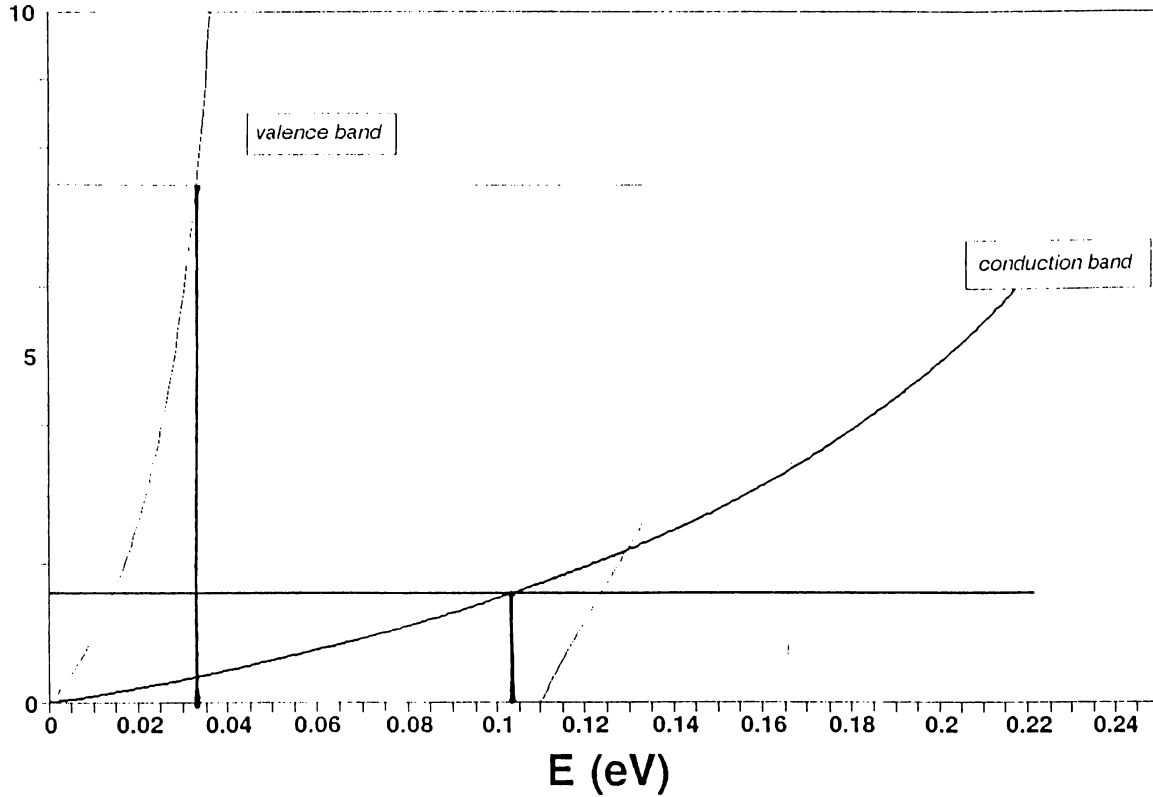


Figure 3.5: Subband Energy Levels of 3.9 nm Quantum Well

The first electron subband level in the conduction band is 103 meV and the first heavy hole level in the valence band is about 27 meV away from the respective band edge.

$$\beta = \sqrt{2m^*(U_o - E)/\hbar^2} \quad (3.22)$$

and the intersection points of either of these equations, in $\alpha a - \beta a$ plane, with the circular arc given as

$$(\alpha a)^2 + (\beta a)^2 = 2m^*U_o a^2/\hbar^2 \quad (3.23)$$

yield the possible energy subband states in the well.¹² The first equation gives odd numbered and the second even numbered levels. Using the relative bandgap offset between GaAs-AlGaAs, which gives the corresponding well depth U_o for conduction and valence bands, and the respective effective masses of the electrons and holes in these bands, m^* , we can obtain both the conduction and valence

band subband energy levels.

For our GRINSCII samples we used a band offset of 0.6/0.4,⁴ i.e. 60% of the total bandgap difference between AlGaAs and GaAs accounts for the conduction band offset and the remaining 40% for the relative valence band difference. The effective mass for electrons in conduction band of GaAs was taken as $0.067 m_0$, where m_0 , is the rest mass of electrons. Similarly the heavy hole mass was taken as $0.48 m_0$ and that of light holes as $0.085 m_0$. The band gaps for AlGaAs and GaAs were calculated from the equation 3.14, taking Al concentration x as 0.3 for AlGaAs at the waveguide-quantum well boundary.

The results show that only one electron subband level exists inside the conduction band of the quantum well and it lies about 103 meV above the conduction band edge of bulk GaAs. Similarly the first heavy hole level lies about 27 meV below the valence band edge whereas the light hole level is 73 meV away from the valence band edge. These values predict that the 1e-1lh transitions, i.e. the transitions between the first electron subband level in the conduction band and the first heavy hole subband level in the valence band, will generate photons of energy around 1.547 eV and the 1e-1lh transitions will be centered around 1.59 eV. No other transitions are expected to be of importance due to the transition selection rules in quantum wells which prohibit, though not strictly in the finite well case, any transitions among levels of different subbands.

However, it should be kept in mind that the calculations made above use a very simplistic model. In reality the nature of these bands is not so simple, in particular the valence bands are notoriously complex. Therefore the above predictions about the transition energies remain a rough estimate at best and especially for the case of 1e-1lh transition a more accurate calculation needs to be done.

3.2.3 Photoluminescence Study

The Photoluminescence spectra of the sample were obtained using a 10 mW He-Ne laser. The wavelength of the laser is 632 nm, and can optically excite

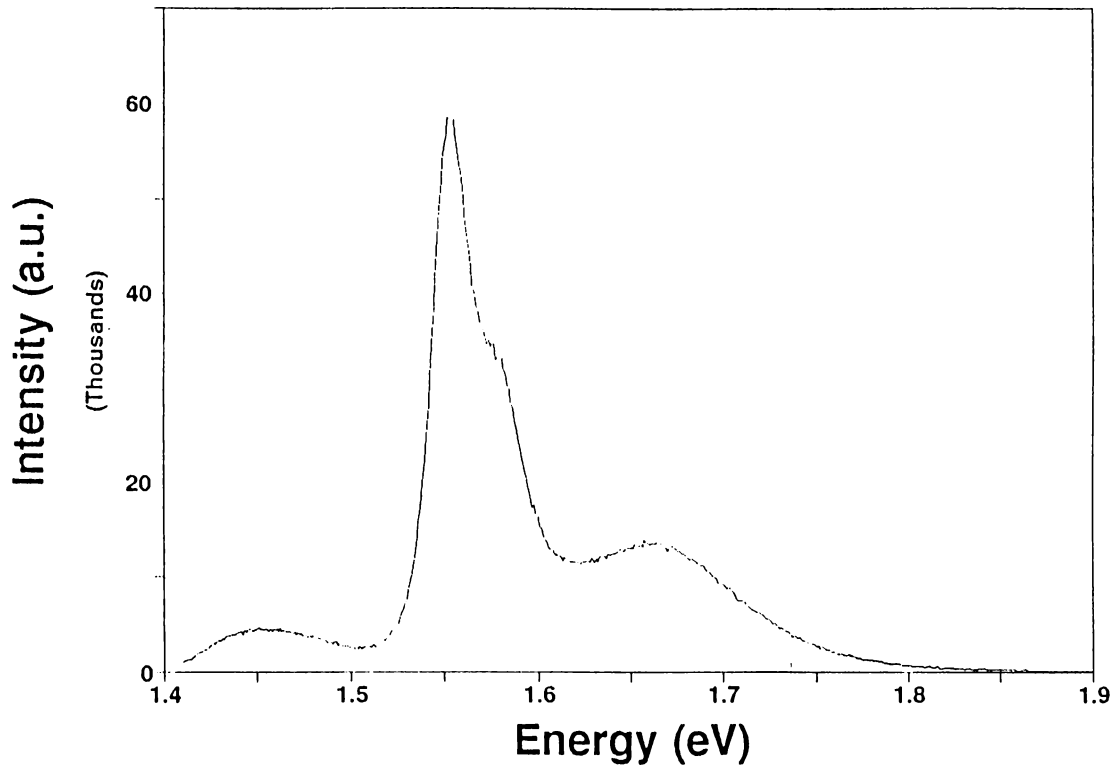


Figure 3.6: PL spectrum from ITO contact Laser

the carriers in the valence band to up to 1.96 eV. At this wavelength, the laser can penetrate easily till the quantum well layer from the p-type $\text{Al}_x\text{Ga}_{1-x}\text{As}$. This laser is therefore sufficient to excite carriers in various quantum well subbands. The spectra was taken using a 1 meter Jobin-Yvon double grating monochromator along with a cooled GaAs photo multiplier and standard photon counting techniques were used. A camera lens with 50 mm focal length was used to focus the signal on the 200 micron wide entrance slit of the spectrometer. The spectra are shown in the Fig.3.6 .

The most striking feature of the PL spectrum is the sharp peak at around 1.55 eV. This peak corresponds to the $1e-1hh$ transitions in the quantum well. A slight shoulder in this peak on the higher energy side, at about 1.575 eV, is due to the $1e-1lh$ transitions in the well. It can be seen that our theoretical prediction of a $1e-1hh$ transition at around 1.547 eV is well satisfied. The model, however, overestimates the $1e-1lh$ transition energy by about 15 meV resulting in about

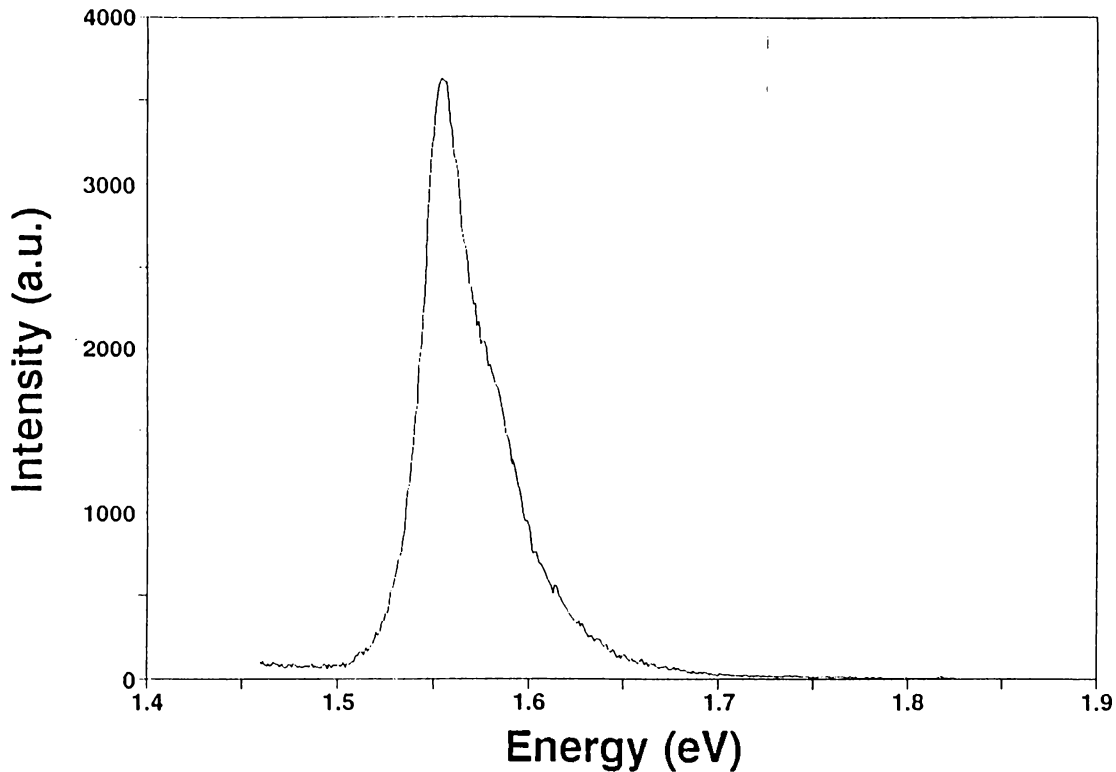


Figure 3.7: EL spectrum from ITO contact Laser at 0.6 mA current

1% of error. Considering the simplification of the model this is acceptable.

There are two other peaks in the PL spectrum. First of these is at energy of around 1.67 eV. This is a broad peak and it is obvious that the light generated in the quantum well can not optically excite this transition which is at higher energy. The other is a relatively weaker peak at around 1.45 eV. We believe that these are impurity related peaks corresponding to the acceptor levels in GaAs for lower energy and in AlGaAs for the higher energy, respectively. We have also looked at an electroluminescence (EL) spectrum of the sample at very low injection, Fig.3.7. The low injection condition is used to avoid the broadening of the quantum well transition peaks. When the two spectra are normalized and compared we see no signs of the peaks at 1.45 eV and at 1.67 eV in the EL spectra. This result shows that both of these peaks are not excited under carrier injection and do not contribute to our unamplified spontaneous emission data.

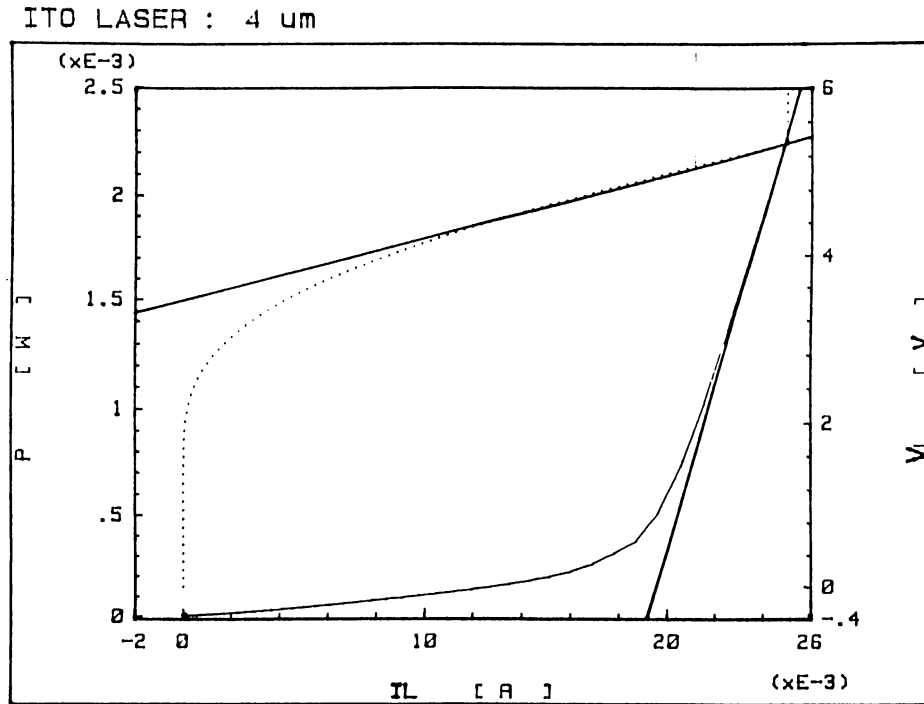


Figure 3.8: I-V and I-P curves For an ITO contact ridge laser. Series resistance R_s and differential quantum efficiency of the lasers can be determined from these curves.

3.3 Characterization of Laser Diodes

The electrical and optical behavior of the laser diodes are evaluated through various parameters such as the threshold current density, differential and internal quantum efficiency, series resistance etc. Two fundamental characteristics of the fabricated lasers were important for our gain measurement work. First of these is the current-voltage behavior of the diodes which gives us the turn-on voltage and series resistance of the lasers. The second main characteristic is the optical output vs. current of the lasers which gives us a knowledge of the threshold current, power of the emitted light and efficiency of the lasers and an estimate of the internal losses of the laser structure. Both of these features are discussed below.

3.3.1 Current-Voltage Characteristics

Functional current-voltage (I-V) tests for the diodes were performed using HP-1112 Modular DC source. In this measurements first the diode characteristic of the lasers were verified. Some of the typical results are shown in Fig.3.8. Under forward bias conditions the current injection is established after a turn-on voltage is achieved and after which a linear increase in the current is observed with increasing voltage. From the slopes of the linear part of the I-V curves the series resistance can readily be deduced. The series resistance of the sample R_s is actually a sum of two parts given as ;

$$R_s = 2R_c + R_b \quad (3.24)$$

where R_c is the specific contact resistance and the second term R_b represents the resistance of the bulk material. Bulk resistance for a slab of a material is given as $R = \rho \frac{l}{A}$ where ρ is the resistivity, l is the length and A is the crosssectional or contact area of the sample. The specific contact resistance R_c can be measured individually by different measuring techniques such as using the Transmission Line Pattern etc.

The measured series resistance of our samples was found to be relatively higher, in the range of 50 to 100 ohms, in comparison to a typical metal alloy contact laser, which are usually a few ohms. This is understandable as we were using the ITO material for our ohmic contacts instead of the generally preferred metal alloy contacts having superior characteristics. Consequently higher driving voltages were necessary for current injection. To avoid heating in the lasers, pulsed modulation of the lasers were chosen. An analysis of optical output of the laser with various duty cycles of pulsed modulation was made to establish an understanding of heating of these lasers with a transition from pulsed to DC biasing. The results are shown in the Fig. 3.9. It can be seen than heating can be avoided if the duty cycle is kept below 0.5% for pulsed modulation.

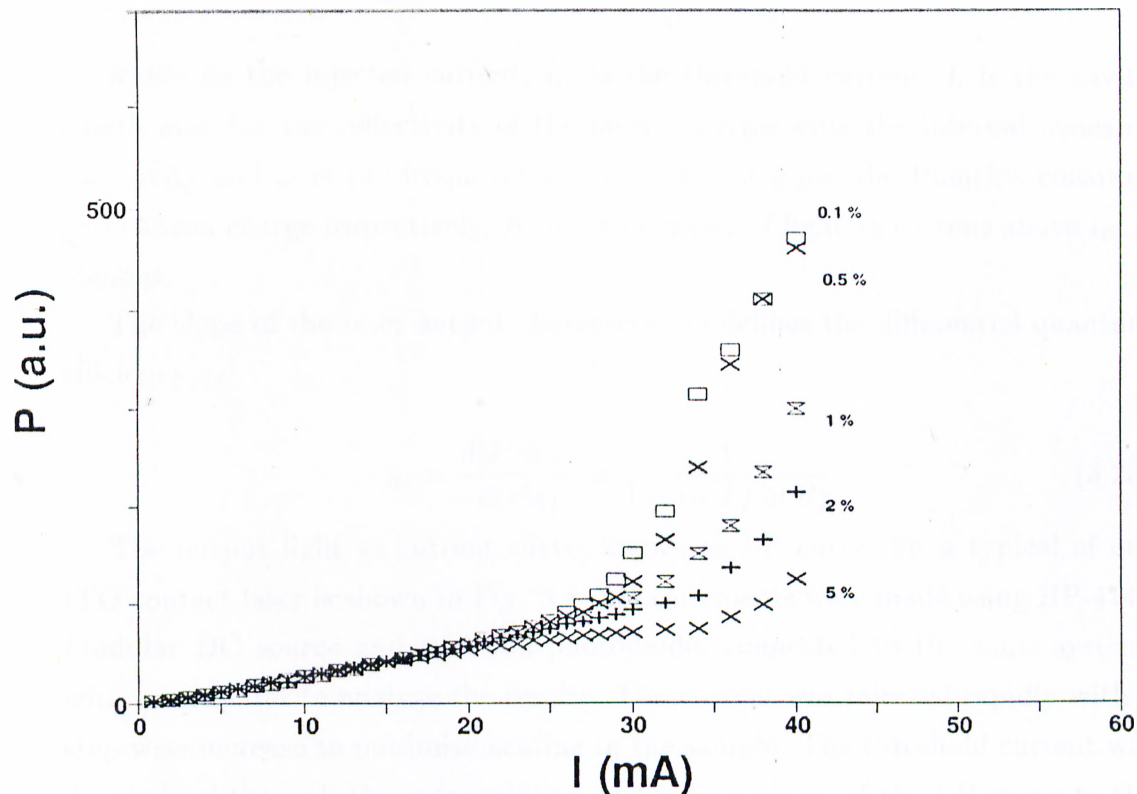


Figure 3.9: Effect of heating on I-P curve of ITO contact lasers
Changes in the I-P curve of an ITO contact laser with an increase in the duty cycle. A drop in differential quantum efficiency of the laser is observed as the duty cycle is increased.

3.3.2 Light Output vs Current Characteristics

In a diode laser, the injection of current leads to the emission of light through spontaneous recombination process first. As the current is increased and the gain of the active medium develops, stimulated emission of light overtakes. The onset of lasing is accompanied by a sharp increase in the emission of light intensity through the facets and beyond this point a linear rise in the output light is observed with an increase in driving current. The value of current at which the lasing begins is called the threshold current of the laser.

The light output power P of the laser through a facet can be given as¹

$$P = \frac{h\nu}{q} (i - i_{th}) \frac{-(1/L) \ln R}{\alpha_i - (1/L) \ln R} \quad (3.25)$$

where i is the injected current, i_{th} is the threshold current, L is the cavity length and R is the reflectivity of the facet. α_i represents the internal losses of the cavity and ω is the frequency of light. h and q are the Planck's constant and electron charge respectively. A linear behavior of light vs current above i_{th} is obvious.

The slope of the laser output characteristics defines the differential quantum efficiency η_d ⁴

$$\eta_d = \frac{d(P/h\omega)}{d(i/q)} = \frac{1}{1 - (\alpha_i L / \ln R)} \quad (3.26)$$

The output light vs current curve, known as I-P curve, for a typical of our ITO contact laser is shown in Fig. 3.8. Measurements were made using HP-4142 Modular DC source and a silicon photodiode, connected to the same system, with a computer to analyze the results. The current was injected rapidly with a step-wise increase to minimize heating in the sample. The threshold current was determined through the extrapolation of the linear part of the I-P curve to the current axis. The slope of this linear part, and hence the differential quantum efficiency of the laser, was calculated for our lasers.

The results show that the threshold current of a typical laser is around 15 to 20 mA. For our 4 μm wide ridge lasers, a cavity length of 530 μm and a threshold current of 17 mA means that the threshold current density is around 0.8 kA/cm^2 . The typical threshold densities of the laser diodes are about^{9,11} 1 kA/cm^2 . The quantum differential efficiencies of our lasers, including emission from both facets, are around 50 to 60 % . Higher efficiencies may be achieved by total elimination of any heating effect which is inevitably present in d.c. biased ITO laser due to its high series resistance.

It should be noted, however, that in the above formulation the contribution of spontaneous emission is neglected. This means that only a fraction of the total photons created goes in to the laser mode. Besides there are non-radiative transitions and leakage currents. Being aware of these effects we may introduce an internal efficiency, η_i , of the laser , so that⁴

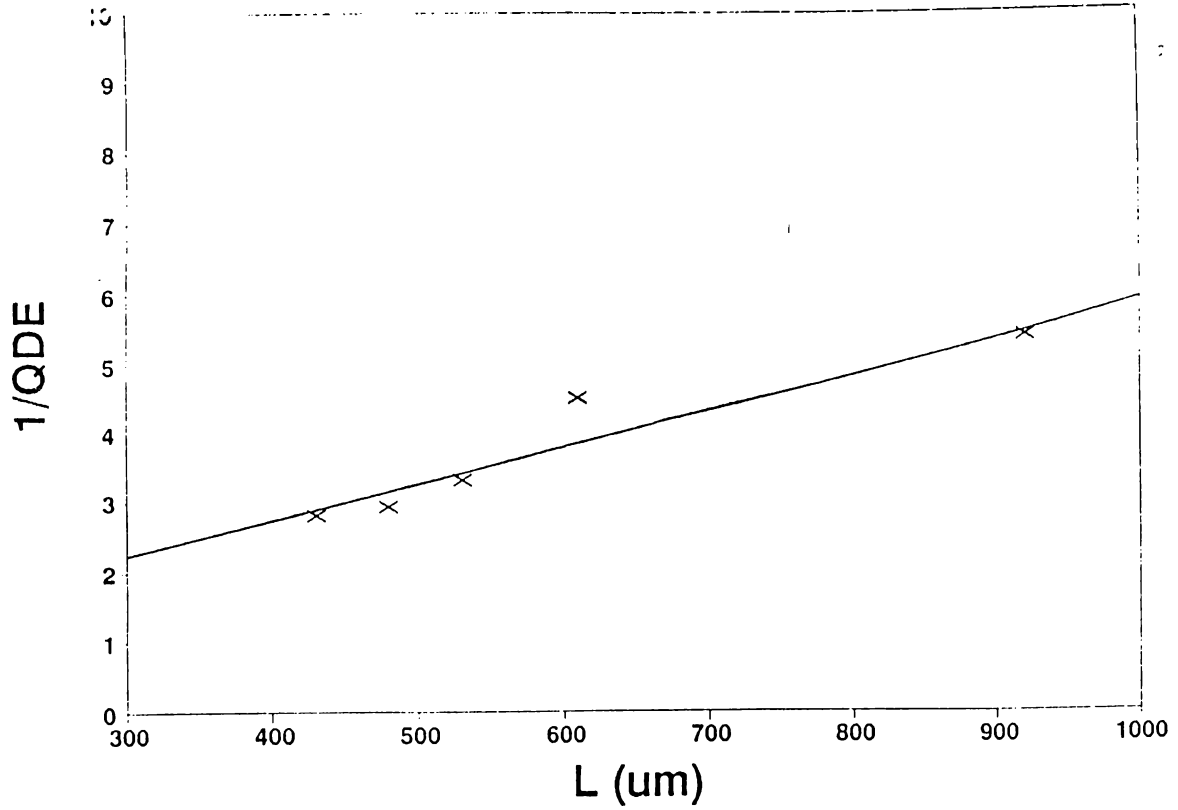


Figure 3.10: Plot of $1/QDE$ vs. L of ITO lasers.
Plot of quantum differential efficiency versus cavity length of ITO contact Lasers

$$P = \frac{\hbar\omega}{q}(i - i_{th})\eta_i \frac{-(1/L) \ln R}{\alpha_i - (1/L) \ln R} \quad (3.27)$$

It then follows that

$$\eta_d = \frac{\eta_i}{1 - (\alpha_i L / \ln R)} \quad (3.28)$$

We may plot the inverse of QD efficiency of the laser against L of lasers, for different cavity length L . The slope of this graph will then yield the internal losses and the intercept will give the internal efficiency. Such a plot for our lasers is shown in Fig. 3.10. It should be noted, though, that the characteristics of two lasers with equal cavity lengths might be vastly different due to several reasons, such as, the mirror quality, ohmic contact quality, non uniformity of the quantum well and other layers in the sample etc. Therefore such an analysis

should be performed with a great number of lasers with a wide range of cavity lengths so that the statistical variations can be minimized.

As a result we may conclude that the typical I-V and I-P characteristics of our lasers are acceptable in general and the values of various parameters are in agreement with the recent results obtained in this field by others.^{4,11}

Chapter 4

Gain Measurements in Laser Diodes

4.1 Introduction

In this chapter we analyze the concept of gain in semiconductor lasers. Following a brief introduction to the idea of gain in such devices, a theoretical model to calculate gain in bulk semiconductors and quantum wells is developed. Beside gain, this theoretical treatment also contains some important concepts necessary to understand the experimental results. Later, two different measurement techniques of gain and their results will be discussed. Beside the fundamental aspects of the development of overall gain under injection of carriers, the nature of spatial variations and the effects of temperature on gain will be assessed.

To understand the concept of gain in a direct bandgap semiconductor we may consider the electronic transitions in a two level system. The valence band and the conduction bands can then be considered as the lower and higher energy levels of the two level system, respectively. Let us consider the electronic transitions, spontaneous and stimulated, between such two energy levels.

With an introduction of radiation in such a system, the electrons may experience an absorption of light and make a transition to upper energy level. The excited electrons in the upper energy level may recombine via either the

spontaneous emission or, under the influence of radiation, stimulated emission. A characteristic feature of such a stimulated transition is that, as regards to its phase, the emitted photon is coherent with the photon that has induced the transition.⁹

Due to the stimulated recombination, the number of photons with a definite energy and phase increases, i.e. a gain of photons is achieved. On the other hand, part of these photons face absorption while travelling in the semiconductor medium, thus defining the loss in the medium. Therefore, in order that the optical amplification shall exceed the absorption, the number of stimulated transitions must be greater than the absorption transitions. In other words, the gain of the system must compensate and overcome the losses. In fact, if we are to use the commonly used notation that the gain can simply be considered as the negative absorption,⁴ we may just say that the total gain of the system, taken as the difference between the losses and amplification in the medium, should be positive.

4.1.1 Methods of Measurement

Several methods have been used to measure gain in semiconductor lasers uptill now. However, two of these methods have been used much more frequently than others. One of these methods was developed by Hakki and Paoli¹³⁻¹⁵ in 1973 in which facet emission of laser devices was used to measure gain. The second method, which is technically easier from the measurement point of view, uses the unamplified spontaneous emission,¹⁶⁻¹⁹ emitted in a direction perpendicular to the cavity axis, to determine gain. We used both of these methods to measure gain in our lasers, and results of both these measurements are discussed below.

4.2 Theoretical Model for Gain

Transitions of the electrons between two energy states E_2 and E_1 , i.e. conduction and valence bands respectively for semiconductors, can result from the emission

or absorption of a photon of energy $\Delta E = h\omega$, where

$$\Delta E = E_2 - E_1 \quad (4.1)$$

One distinguishes three elementary processes : absorption, stimulated emission and spontaneous emission. For absorption the spectral transition rate $r_{12}(h\omega)d(h\omega)$, i.e. the number of transitions per unit volume and time in the energy interval $d(h\omega)$ around the photon energy $h\omega$, depends on the photon density $\rho_s(h\omega)d(h\omega)$ in the relevant photon energy interval and on the densities of the initial states E_1 and end states E_2 as well as the probabilities that the initial state is occupied and the end state is unoccupied. In semiconductor lasers the injection of carriers in an otherwise unperturbed semiconductor in its equilibrium condition changes the equilibrium concentration of carriers in the conduction and valence bands. The intraband relaxation time of energetic carriers inside the conduction or valence bands, though, are much smaller than the interband transition lifetimes.^{20,21} The carriers therefore come to a quasi equilibrium condition within a band before recombination.^{22,23} The occupation probability of an energy state E within these bands under such quasi-equilibrium condition can then be expressed in terms of the Fermi distribution function given as⁴

$$f_{c,v}(E) = (1 + \exp(\frac{E - E_{F_{c,v}}}{kT}))^{-1} \quad (4.2)$$

where $E_{F_{c,v}}$ is the quasi Fermi energy and subscripts c and v represent the conduction and valence bands, respectively.

Hence, the total spectral absorption rate between any two energy states obeying the condition $E_2 - E_1 = h\omega$, is given as

$$r_{12}(h\omega)d(h\omega) = B_{12}(h\omega)\rho_s(h\omega)d(h\omega) \int_{-\infty}^{\infty} D_c(E_1+h\omega)(1-f_c(E_1+h\omega))D_v(E_1)f_v(E_1)dE_1 \quad (4.3)$$

where $D_{c,v}$ are the densities of states in conduction and valence bands. f_v represents the probability that the valence band state is filled and $(1 - f_c)$

represents the probability that the conduction band state is empty. The proportionality constant B_{12} is called the Einstein coefficient for absorption. By analogy a similar expression for the spectral stimulated emission rate is found to be

$$r_{21}(h\omega)d(h\omega) = B_{21}(h\omega)\rho_s(h\omega)d(h\omega) \int_{-\infty}^{\infty} D_c(E_1+h\omega)f_c(E_1+h\omega)D_v(E_1)(1-f_v(E_1))dE_1 \quad (4.4)$$

where B_{21} is the Einstein coefficient for stimulated emission.

In addition to stimulated emission and absorption there are also spontaneous transitions from the conduction band to the valence band, which tend to restore thermodynamic equilibrium even without external radiation. With the introduction of the Einstein coefficient A_{21} for spontaneous emission, the spectral spontaneous emission rate may be written as

$$r_{sp}(h\omega)d(h\omega) = A_{21}(h\omega)d(h\omega) \int_{-\infty}^{\infty} D_c(E_1+h\omega)f_c(E_1+h\omega)D_v(E_1)(1-f_v(E_1))dE_1 \quad (4.5)$$

To determine the distribution of photon energies in a semiconductor we note that possible states for photons are found only at frequencies such that standing electromagnetic waves form in the semiconductor volume. This is in complete analogy with the possible electron states in a crystal. The occupation probability of the states in thermodynamic equilibrium for photons is given by the Bose-Einstein distribution given⁴ as $f_{ph} = (\exp(\frac{h\omega}{kT}) - 1)^{-1}$.

Calculation of the density of states, and assuming the medium to be non-dispersive, then leads to the Planck's law which gives the spectral photon density $\bar{\rho}_s$ as

$$\bar{\rho}_s(h\omega)d(h\omega) = \frac{\bar{n}^3}{\pi^2 h^3 c^3} \frac{(h\omega)^2}{\exp(\frac{h\omega}{kT}) - 1} d(h\omega) \quad (4.6)$$

where the spectral photon density $\bar{\rho}_s(h\omega)$ indicates the number of photons per unit volume and energy interval.

The requirement that there is equilibrium in detail, so that the emission and absorption rates at each photon energy exactly compensate each other, i.e.

$$r_{12}(h\omega) = r_{21}(h\omega) + r_{sp}(h\omega) \quad (4.7)$$

then gives the well known relations between different Einstein coefficients, given as

$$B_{12} = B_{21} \quad (4.8)$$

and

$$A_{21} = \frac{\bar{n}^3}{\pi^2 h^3 c^3} (h\omega)^2 B_{21} \quad (4.9)$$

These relation still remain valid even if the coefficients B_{12} , B_{21} and A_{21} depend on the photon energy. The above relation means that the transition probability for absorption and stimulated emission are equal while the probability of spontaneous emission increases in comparison with that of stimulated emission, as the photon energies are increased.

We now consider a plane wave of frequency $\omega = (E_2 - E_1)/h$ as it passes through a semiconductor. Absorption will cause a decrease in the number of photons in the wave and the stimulated emission will increase their number. Spontaneous emission takes place equally in all directions, and only a small fraction of this contribution of photons will proceed (with random phase) in the direction of the incident plane wave. We may therefore assume that the change in spectral photon density can be given as

$$\frac{d\rho_s}{dt} = r_{21} - r_{12} \quad (4.10)$$

where $(r_{21} - r_{12})$ is the net absorption rate. Letting the propagation of the wave in x-direction, the well known Lambert-Beer's law gives

$$\frac{d\rho_s}{dx} = -\alpha\rho_s(x) \quad (4.11)$$

The absorption coefficient $\alpha = \alpha(h\omega)$ characterizes the decrease of the photon density with x . Since the photons move with the group velocity v_g , we may set $dx = v_g dt$ and obtain

$$\alpha \rho_s v_g = r_{21} - r_{12} \quad (4.12)$$

Substitution of the rates 4.3 & 4.4 and using the equation 4.9, for a non dispersive medium with $v_g = c/\bar{n}$, we obtain

$$\alpha(h\omega) = \frac{\hbar \lambda^2}{4\bar{n}^2} A_{21}(h\omega) \int_{-\infty}^{\infty} D_c(E_1 + h\omega) D_v(E_1) [f_v(E_1) - f_c(E_1 + h\omega)] dE_1 \quad (4.13)$$

According to this relation if, for all values of E_1 , $f_v(E_1)$ is smaller than $f_c(E_1 + h\omega) = f_c(E_2)$, then α is certainly negative. This implies amplification of photons. This condition is the well known condition of inversion of population needed for amplification in lasers. This condition is equivalent to saying that for a photon of energy $h\omega$ to experience amplification, it must satisfy the condition

$$E_g < h\omega < E_{fc} - E_{fv} = \Delta E_f \quad (4.14)$$

This is the famous Bernard-Duraffourg condition. The energy gap E_g is the band gap energy for bulk systems and the difference between the subband energy levels for quantum wells. Two important conclusions are drawn from this condition : (1) Amplification in a system will start only when the quasi Fermi level separation is greater than the energy gap E_g . (2) Only the photons with energy less than ΔE_f may be amplified. The carrier density required to create a ΔE_f equal to E_g in a system is called the transparency density N_{tr} and is directly related to the density of states in a system.

An attempt to calculate gain directly by using above relation for absorption leads to inexact results when compared with the experimental data.⁴ The reason for this discrepancy is the failure to take into account the k -momentum conservation in the electron transitions. The selection rule appears in full rigor for the direct bandgap semiconductors such as GaAs. Due to this rule, of all

the energetically possible transitions, only one subgroup of transitions is selected. The relations between the Einstein coefficients though remain unaltered when the selection rule is taken into account and the connection between the spontaneous emission spectrum and the absorption coefficient remains immune to this rule as well.⁴ However, to calculate gain theoretically this rule must be taken into account and leads to a slightly different expression for absorption coefficient than the one derived earlier.

The calculation of absorption and amplification requires a determination of transition probabilities of the electrons in the presence of electromagnetic radiation. This treatment can be found in nearly all books on quantum mechanics. The Hamiltonian operator in the general case of an electron in electromagnetic field can be given as ,

$$H = H_0 + \frac{iq\hbar}{m_0} A \cdot \nabla \quad (4.15)$$

where $H_0 = \frac{p^2}{2m_0} + U(r)$ and A is the magnetic vector potential which defines the magnetic field $\tilde{B} = \nabla \times A$. The second term on the right side of the expression can be considered as the perturbation term for the Hamiltonian giving

$$H = H_0 + H' \quad (4.16)$$

Using the time dependent Schrodinger equation and defining Ψ_m as the orthonormal eigenfunctions of unperturbed Hamiltonian H_0 , with eigenenergies E_m , we may express the eigenfunction Ψ of Hamiltonian H as

$$\Psi(x, y, z, t) = \sum_m a_m(t) \exp\left\{\frac{-iE_m t}{\hbar}\right\} \Psi_m(x, y, z) \quad (4.17)$$

The square of the modulus $|a_m(t)|^2$ represents the probability that the system finds itself in the eigenstate Ψ_m . This analysis then leads us to the famous Fermi's Golden Rule, given as

$$P_{mj} = \frac{2\pi}{\hbar} |\hat{H}'_{jm}|^2 \delta(E_j - E_m + \hbar\omega) \quad (4.18)$$

where P_{mj} is the transition rate from state m , with energy E_m , to state j , with energy E_j , and \widehat{H}'_{jm} is the so-called matrix element defined by

$$H'_{jm} = \int \Psi_j^* H' \Psi_m dr^3 \quad (4.19)$$

The delta function allows only the transitions between energy levels having an energy difference of $h\omega$. This calculated transition rate evidently is valid for absorption and stimulated emission processes. Spontaneous emission which takes place in all directions, cannot be treated within this framework. Another limitation of Fermi's Golden Rule is that it assumes that only very few electrons are removed by radiation from their initial states because only first order terms in the perturbation theory are taken into account.

The perturbation portion of the Hamiltonian operator for a linearly polarized plane wave, travelling in the z -direction, can be written as

$$H'(t) = \frac{E_y q \hbar}{m_0 \omega} \exp(i\beta z) \exp(-i\omega t) \frac{\partial}{\partial y} + \frac{E_y^* q \hbar}{m_0 \omega} \exp(-i\beta z) \exp(i\omega t) \frac{\partial}{\partial y} \quad (4.20)$$

Therefore the energy matrix element $|\widehat{H}'_{21}|^2$ for a transition from $m = 1$ to $j = 2$ is

$$|\widehat{H}'_{21}|^2 = \frac{|\widehat{E}_y|^2 q^2}{m_0^2 \omega^2} \left| \int \Psi_2^* \frac{\hbar}{i} \left(\frac{\partial}{\partial y} \Psi_1 \right) \exp(i\beta z) dr^3 \right|^2 \quad (4.21)$$

which allows us to define the momentum matrix element of the transition as

$$M_{21} = \int \Psi_2^* \frac{\hbar}{i} \left(\frac{\partial}{\partial y} \Psi_1 \right) dr^3 \quad (4.22)$$

In the semiconductors the transitions occur between valence bands and the conduction bands so that the states 1 and 2 can be replaced by conduction band energy E_c and the valence band energy E_v . The net transition rate, i.e. the difference between absorption and stimulated emission ($P_{vc} - P_{cv}$), can then be written as

$$P(\hbar\omega) = \frac{1}{2\pi^2\hbar} \int_{-\infty}^{\infty} \left| \widehat{M}_{cv}(k) \right|^2 [f_v(1-f_c) - f_c(1-f_v)] \delta(E_c(k) - E_v(k) - \hbar\omega) dk^3 \quad (4.23)$$

where, introducing the conservation of momentum, we have assumed that $k = k_c = k_v$, as the contribution of the momentum of photons in the transition is negligibly small. $f_{c,v}$ are the quasi Fermi distribution of carriers in the conduction and valence bands. We have also taken $|\widehat{M}_{cv}| = |\widehat{M}_{vc}|$. For parabolic bands we have

$$E_c(k) - E_v(k) = \frac{\hbar^2 k^2}{2} \left(\frac{1}{m_c} + \frac{1}{m_h} \right) + E_g \quad (4.24)$$

where E_g is the band gap and m_c and m_h are the effective masses for electrons and holes, respectively, in the conduction and valence bands. The wavefunctions of the carriers in the semiconductor are Bloch waves of the form

$$\Psi_{c,v}(r) = \frac{1}{\sqrt{V_k}} u_{c,v}(k_{c,v}, r) \exp\{ik_{c,v}r\} \quad (4.25)$$

Using these wavefunctions the matrix element for a linearly polarized plane wave can be found to be

$$\left| \widehat{M}_{cv}(k) \right|^2 = \frac{q^2}{m_0^2 \omega^2} \left| \widehat{E}_y \right|^2 |M_{cv}(k)|^2 \quad (4.26)$$

We have so far assumed that the k-conservation in the electron transitions is exact. This is expressed by the δ function in the transition rates $P(\hbar\omega)$. However, the finite lifetime of the electrons in the bands leads to a deviation from the strict selection rule and to a spectral broadening. The δ function is then usually replaced by a Lorentzian-type broadening function

$$L(E_c(k) - E_v(k) - \hbar\omega) = \frac{\hbar/(\tau_{in}\pi)}{(E_c(k) - E_v(k) - \hbar\omega)^2 + (\hbar/\tau_{in})^2} \quad (4.27)$$

which is characterized by the intraband relaxation time τ_{in} . The absorption coefficient for transitions in a bulk semiconductor can then be shown to be

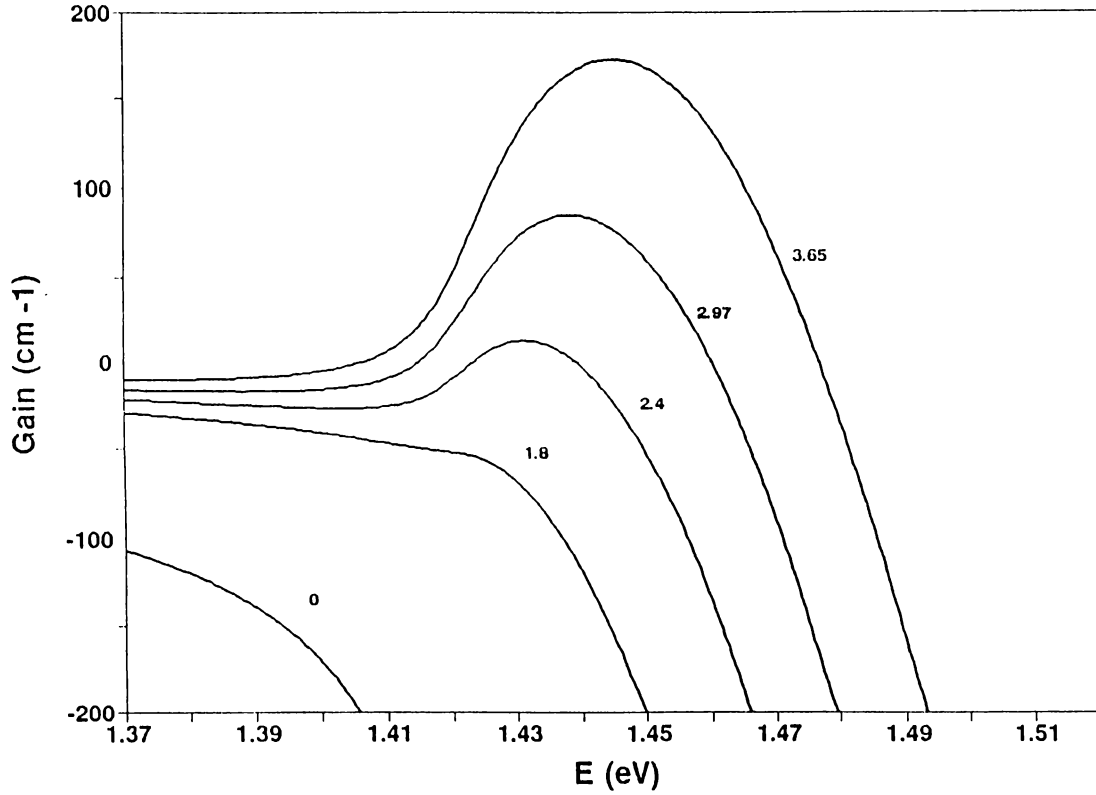


Figure 4.1: Calculated Gain in Bulk GaAs

The calculated gain for bulk GaAs at different injected carrier densities. Carrier densities are in 10^{18} cm^{-3}

$$\alpha(h\omega) = \frac{q^2}{\bar{n}cc_v(2\pi)^2m_0^2\omega} \int_{-\infty}^{\infty} |M_{cv}(k)|^2 [f_v(E_v(k)) - f_c(E_c(k))] L(E_c(k) - E_v(k) - h\omega) dk^3 \quad (4.28)$$

In quantum well the continuous energy subbands assume discrete energy values in one of the space direction, say x-direction. The momentum vector for a subband state with energy E_ν , therefore takes discrete values in x-direction as well, given by $k_\nu = (k_{x\nu}, k_y, k_z)$. Transitions take place between energy subbands of the same order in the conduction band, $E_{c\nu}$, and the valence bands, $E_{v\nu}$. A similar argument then leads to the absorption coefficient in the quantum wells, given as

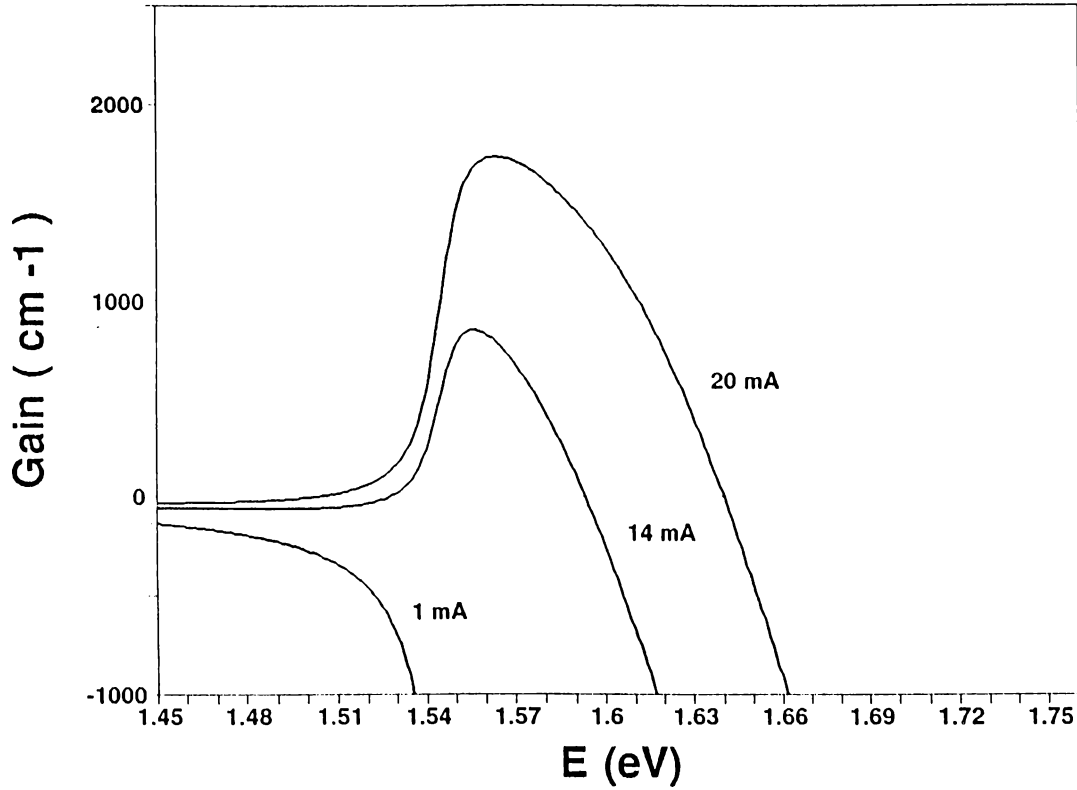


Figure 4.2: Calculated Gain in GaAs Quantum Well

The calculated gain for 3.9 nm, undoped, GaAs quantum well at different injected currents.

$$\alpha(\hbar\omega) = C \sum_{\nu} \int_{-\infty}^{\infty} |M_{c\nu}^{\nu}(k_{\nu})|^2 [f_{\nu}(E_{c\nu}(k_{\nu})) - f_c(E_{c\nu}(k_{\nu}))] L(E_{c\nu}(k_{\nu}) - E_{v\nu}(k_{\nu}) - \hbar\omega) k' dk' \quad (4.29)$$

where $C = q^2 / (\bar{n} c c_{\nu} m_{\nu}^2 \omega a_x)$, a_x is the thickness of the quantum well, $(k')^2 = k_y^2 + k_z^2$ and $k_{\nu}^2 = k_{x\nu}^2 + k_y^2 + k_z^2$.

The above two relations can therefore be used to theoretically determine the gain in bulk semiconductors and quantum well structures.

The gain calculated using equation 4.28 for bulk GaAs has been shown in Fig. 4.1. It can be seen that the peak gain is on the order of a few hundred of cm^{-1} . This is quite low compared to the quantum well gain. In Fig. 4.2 the gain calculation for a 3.9 nm GaAs quantum well is shown. The variation in quantum

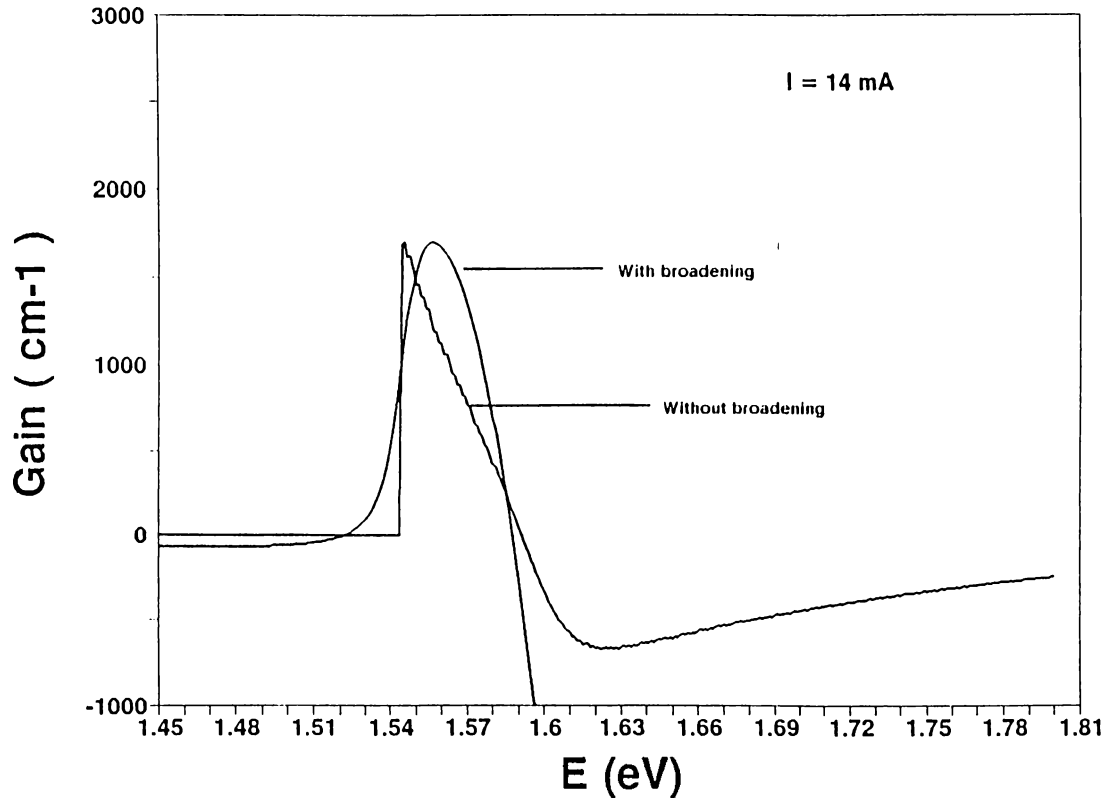


Figure 4.3: Broadening in QW gain spectrum

The calculated gain for GaAs quantum well, with and without the intraband relaxation broadening scheme.

well gain due to the broadening is shown in Fig. 4.3 .

The use of Lorentzian lineshape function is common²⁴; more recently,^{25,26,20} however, more sophisticated line shape functions have been derived. For example, Yamanishi and Lee have suggested^{27,28} that the state decays initially as a Gaussian but then takes on exponential behaviour for larger times. Asada²⁹ has arrived at an asymmetrical lineshape function that falls off much faster than a Lorentzian on the low energy side of the transition, similar to what Yamanishi and Lee have found. Kucharska and Robbins²⁴ have suggested the use of an energy-dependent lifetime. Rees et al⁷ have recently suggested the introduction of separate line broadening functions for conduction and valence band states. At present there appears to be no consensus as to which lineshape most closely resembles reality.

4.3 Hakki-Paoli Method

This is a method of deriving gain spectrum of a laser below threshold by observing the magnitude of the Fabry-Perot resonances of the longitudinal modes. It is shown by Thompson¹ that the ratio ρ between any intensity maximum of the longitudinal modes spectrum P^+ and the nearby intensity minimum P^- can be given as

$$\rho = \frac{P^+}{P^-} = \left\{ \frac{1 + R \exp[(g - \alpha)L]}{1 - R \exp[(g - \alpha)L]} \right\}^2 \quad (4.30)$$

where L is the length of the cavity, g is the modal gain and α represents the internal loss of the laser. Modal gain is the gain experienced by a specific transverse mode in the laser.⁹ As our sample structure allows only the fundamental transverse mode to exist in the active region the above expression applies to this zeroth order mode. R is the reflectivity of the mirrors where, for the sake of simplicity, the reflectivities R_1 and R_2 of the two mirrors have been taken to be equal. The ratio ρ may be replaced by a depth of modulation parameter r which at any given wavelength is the ratio of the average of two consecutive peaks ($\frac{P_i^+ + P_{i+1}^+}{2}$) to the intermediate valley or the intensity minima P_i^- , so that

$$r_i = \frac{P_i^+ + P_{i+1}^+}{2P_i^-} \quad (4.31)$$

Hence, the net gain ($g - \alpha$) is given in terms of r_i by

$$(g - \alpha) = \left(\frac{1}{L}\right) \ln \left\{ \frac{\sqrt{r_i} - 1}{\sqrt{r_i} + 1} \right\} + \frac{1}{L} \ln \left(\frac{1}{R}\right) \quad (4.32)$$

Here the first term on the right hand side represents the contribution from the modulations and the second term is the constant cavity loss.

This relationship thus provides the means for experimentally deriving net gain in a laser as a function of injection current up to the threshold current of the laser and as a function of wavelength over some fraction of the spontaneous emission linewidth.

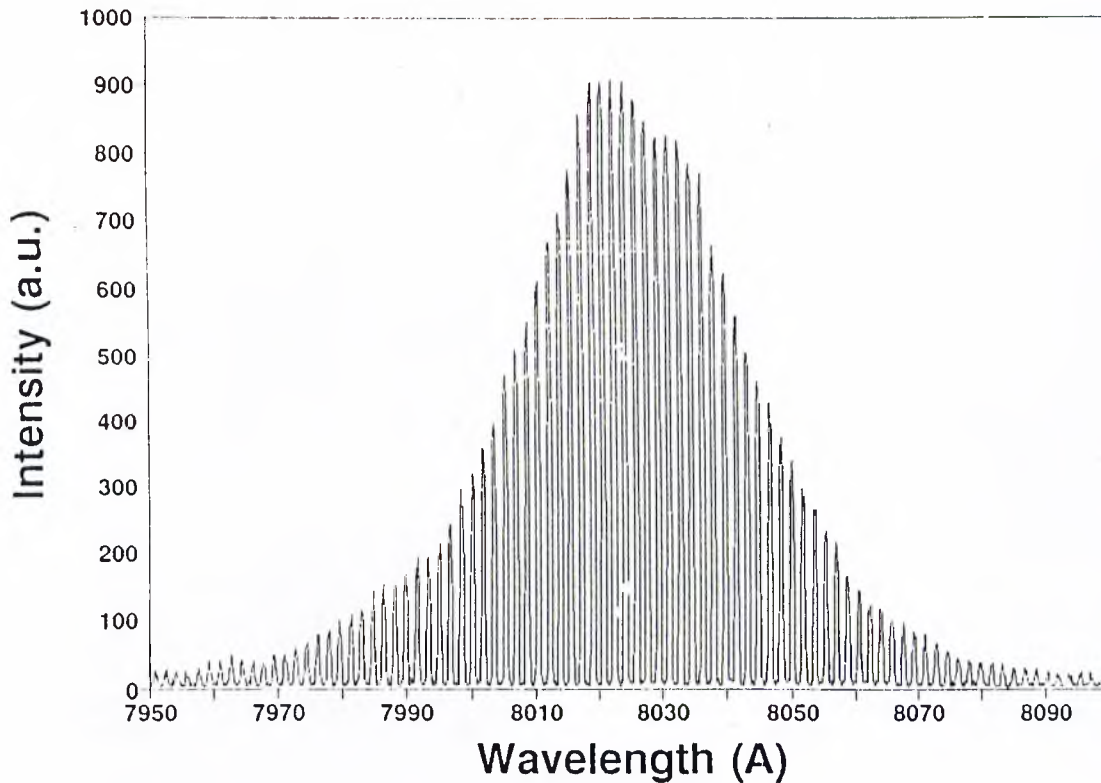


Figure 4.4: Spontaneous Emission Spectrum from Facet
The longitudinal mode spectra of a laser at 12 mA current. Threshold current of the laser is 16 mA.

4.3.1 Measurement Setup and Results

To measure gain of our ITO contact lasers by Hakki-Paoli method we used a 1 meter Jobin Yvon double grating monochromator. Light emitted from the facet of the laser was directed to the entrance slit of the monochromator using a microscope objective. The laser was placed in such a way that the plane of the quantum well layer remained perpendicular to the entrance slit. The image of our $4 \mu\text{m}$ ridge of the laser was magnified by 30 times and the entrance slit of the monochromator was set to $5 \mu\text{m}$. Thus light from an area of about $0.2 \mu\text{m}$ of the whole ridge was collected. Laser was pumped by pulse Hewlett and Packard pulse generator. To avoid heating in the sample, the pulse frequency was kept to 1 kHz and the pulse width to $2 \mu\text{s}$, giving a duty cycle of 0.2 %. The current in the laser was monitored using a current probe and an oscilloscope.

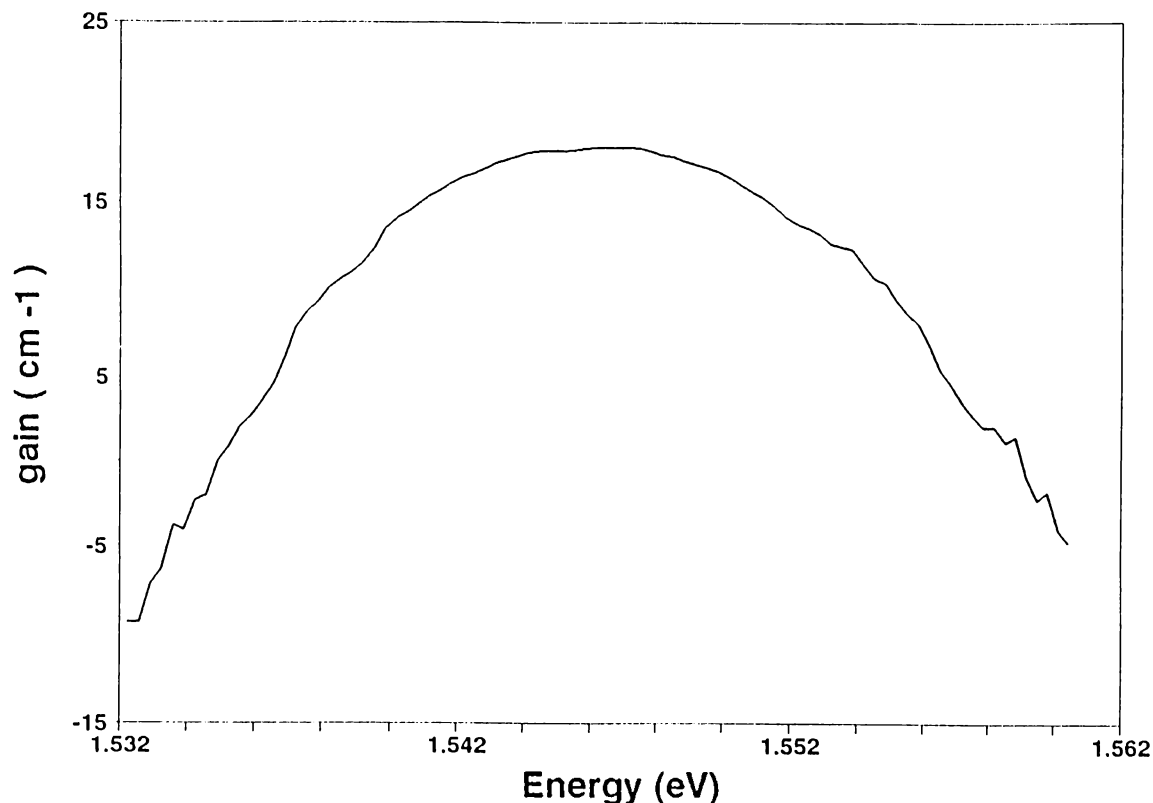


Figure 4.5: Net Gain

Net gain, $(g - \alpha)$, of ITO contact laser at 12 mA current.

An example of the data thus obtained from a laser at 12 mA of current is shown in Fig. 4.4. This laser had a cavity length of 520 μm and threshold current is 16 mA. The counting time for the signal was 1 second for each data point and the interval between two consecutive points was kept to 0.01 nm to resolve the peaks and the valleys of the resonance modes spectra.

The peak of the emission spectra occurs at around 802 nm. The signal then sharply decreases on either side of the peak point and about 7 to 8 nm away from the peak the signal reduces to less than 5 % of its peak value. As can be seen in the Fig. 4.4, the overall width of the spectra is quite narrow and on energy scale spans a range of less than 35 meV. The spacing between two consecutive peaks of the spectra is seen to be about 1.8 Angstrom. This value is in accordance with the relation established earlier between the longitudinal mode spacing and the length of the laser cavity.

Using the equation 4.32 the data was then converted to yield the net gain of this laser. The value of R was taken to be 0.32 . The results are shown in Fig.4.5. It can be seen that the peak value of gain is about 18 cm^{-1} . Though the gain of a laser is inherently dependent on the sample characteristics and device structure, our results, are in accordance with the results obtained previously by others for similar devices.³⁰ As can be seen from the equation 4.32 , the net gain is inversely proportional to the length of the cavity and for higher values of gain a shorter cavity laser should be used.

As the current in the laser is increased towards the threshold current value the net gain ($g - \alpha$) tends to the cavity loss limit, or in other words, the gain g tends to the threshold gain limit. Rewriting equation 4.32 as

$$g = \left(\frac{1}{L}\right) \ln\left\{\frac{\sqrt{r_i} - 1}{\sqrt{r_i} + 1}\right\} + \alpha - \frac{1}{L} \ln\left(\frac{1}{R}\right) \quad (4.33)$$

we can see that if the first term on the right side becomes zero the expression for gain reduces to the g_{th} . As the threshold current is approached the intensity of the lasing mode increases rapidly and at the onset of lasing its magnitude becomes several times greater than nearby modes. This effect for our laser has been shown in the Fig.3.4. This tremendous rise in the intensity of lasing mode increases the depth of modulation parameter r_i , thus diminishing the contribution from the first term on the right side of the equation 4.33. Hence the gain g approaches its threshold limit g_{th} . In the limit when the modulation parameter is increased to ∞ , the first term disappears altogether. This phenomena also sets an upper limit for the net gain ($g - \alpha$) as $\frac{1}{L} \ln R$, known as the mirror loss. The value of mirror loss for our laser under consideration is about 21.9 cm^{-1} .

The feature of the gain curve around the peak value is very smooth but at the high and low wavelength limits it drops off quite rapidly. At the high energy side of the emission spectrum, the quasi Fermi level separation limit is approached. Beyond this limit the gain should become negative as only the absorption can occur in this region.^{24,31} This effect is seen in our gain spectrum where on the higher energy side, the gain makes a transition from positive to negative values.

At the low energy side of the emission spectrum the band edges of the

conduction and valence bands are approached and the density of states vanishes in the forbidden band gap region. Therefore the gain, g , should tend to zero and the measured net gain value should tend to $-\alpha$. From our data the value of α was estimated to be about 7cm^{-1} . Though the magnitude of loss is usually a parameter specific to a laser, this value is quite consistent with the results previously reported.³⁰ However, it should be kept in mind that during the acquisition of data, inclusion of some noise is inevitable and results in the fluctuations in the gain curves. The effect becomes more prominent as the signal deteriorates and can be compensated for by increasing the signal counting time of the photomultiplier, thus increasing the signal to noise ratio at the cost of much longer data acquisition times.

Besides modal gain the concept of material gain is of fundamental importance as well in the laser devices. Material gain in the quantum well lasers is an indication of the quality of the quantum well structure. The difference between modal and material gain can be understood as follows. The light wave generated in the active region propagates not only in the active zone but also penetrates into the immediate surroundings. The thinner the active layer is, the deeper is the penetration in the adjacent layers. This means that a portion of the created photons no longer take part in the feedback mechanism of the laser. The modal confinement factor Γ indicates the fraction of the light intensity of a mode which is guided in the active zone and takes part in the stimulated emission. The modal gain for a transverse mode is obtained by multiplying the material gain by the confinement factor Γ . Therefore the material gain of our laser can be found by dividing the net gain $(g - \alpha)$ calculated earlier by Γ . Denoting the material gain as G , we then get⁴

$$G = \frac{\alpha}{\Gamma} + \left(\frac{1}{\Gamma}\right)\left(\frac{1}{L}\right) \ln\left\{\frac{(r_i^{1/2} - 1)}{R(r_i^{1/2} + 1)}\right\} \quad (4.34)$$

Thus to calculate the material gain using the Hakki Paoli technique, we need to know the confinement factor for the fundamental transverse mode for our laser structure and the internal losses α . For a perfect confinement of the optical mode

in the active region the value of Γ is one but in actual lasers the confinement factor is usually far below one, especially for the thin active region quantum well lasers. It has been shown⁴ that the value of the confinement factor Γ for a GaAs/AlGaAs GRINSCHE quantum well system with a parabolic profile can be obtained, to a good approximation, using the relation

$$\Gamma = \sqrt{\frac{2}{\lambda D}} d (n_f^2 - n_s^2)^{\frac{1}{4}} \quad (4.35)$$

where d and D are the thicknesses of the active and waveguide layers respectively. n_f and n_s are the refractive index at the center and edge of the parabolic waveguide region. For our lasers n_f was found to be 3.3852 for an aluminum concentration of 30% at the waveguide-active region boundary. Similarly at the cladding-waveguide boundary n_s was calculated to be 3.1968 for a 60% aluminum ingredient in AlGaAs. Taking the active region thickness to be 3.9 nm and that of waveguide layer as 200 nm the confinement factor turns out to be about 0.02. The value of α was taken to be 7 cm^{-1} . Using the equation 4.34 the data was converted to obtain material gain of the laser and the results are shown in Fig.4.6.

The profile of the material gain curve is very similar to the modal gain curve. The peak material gain magnitude, though, is about 1200 cm^{-1} as compared to the peak modal gain value of about 18 cm^{-1} . At the low energy end of the gain curve the material gain tends to zero just like the modal gain g . Though the basic trend is obvious, the exact crossover to negative gain values at the high energy end is not clear in the Fig.4.6. This is due to the limitations put by poor signal in this region of the spontaneous emission spectrum. If the mode spectrum is made to extend further towards higher energy side the material gain obtained from the curve will be seen to take the negative values after the quasi Fermi level separation limit.

Another feature of gain in the laser is its development in relation to the increase in the injection current. The net gain curves for three different current levels are shown in the Fig.4.7. As the current is increased from 8 mA to 12 mA, the profile of the gain curve changes. First of all, the peak gain increases as

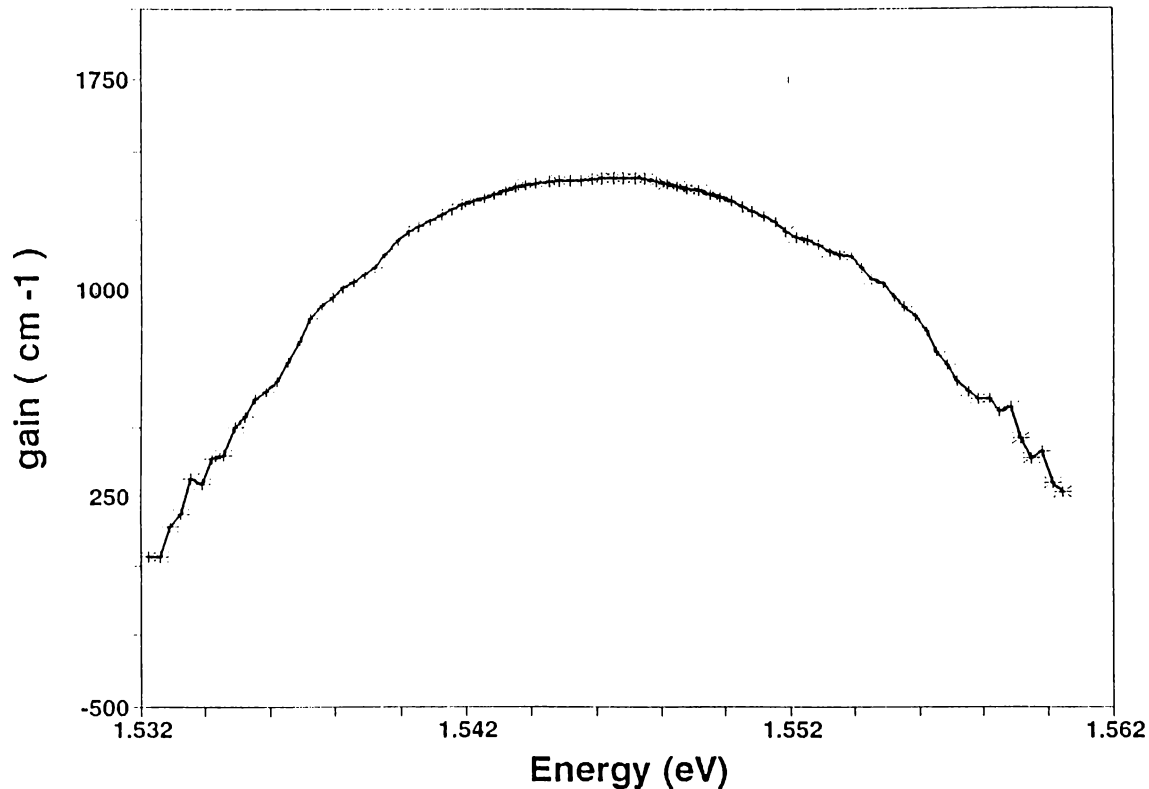


Figure 4.6: Material Gain

Material Gain of the ITO laser at 12 mA current.

the current is increased. This increase in the peak gain is accompanied by a shift towards higher energies. In addition, the whole gain curve becomes increasingly broader as the current is increased. The crossover point to negative values of gain at higher energy side also shifts with increasing current. All these effects are due to the band filling and will be considered in more detail later on. The gain curves, though, seem to converge towards a single point on the lower energy end of the spectra. This corresponds to the internal loss α of the laser as pointed out earlier.

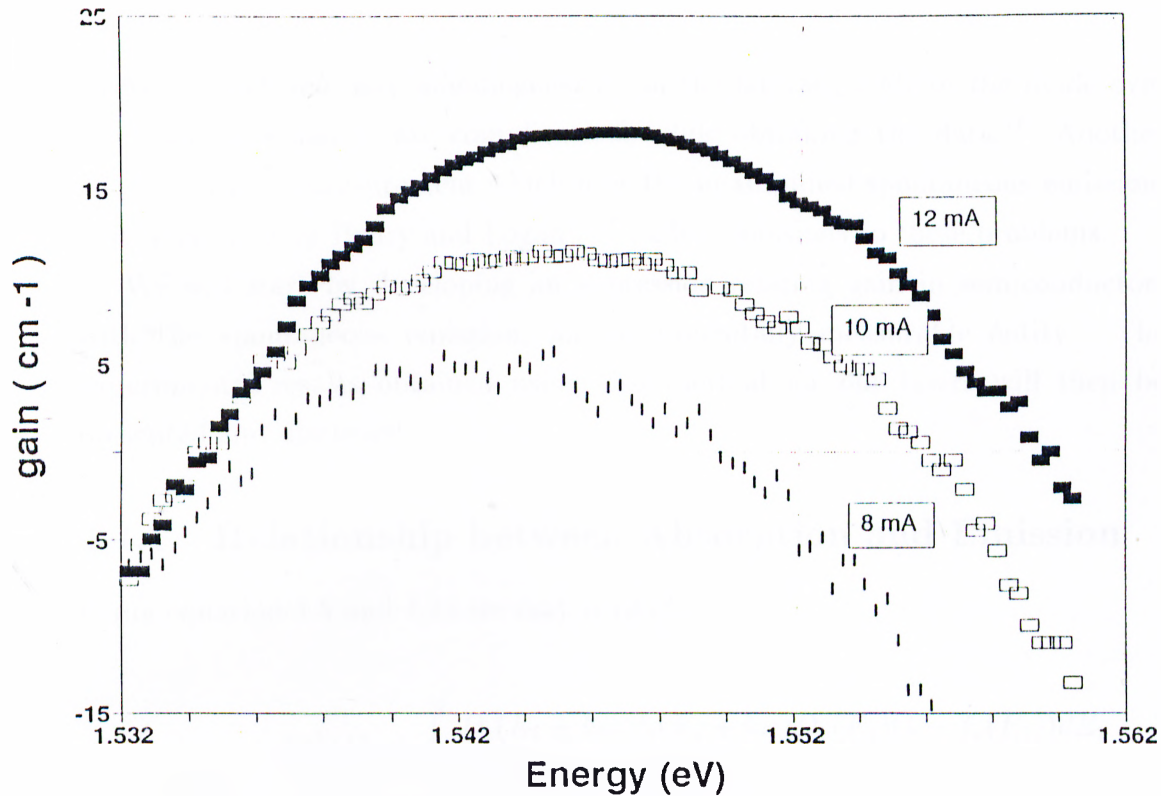


Figure 4.7: Gain vs. Current

The development of net gain ($g - \alpha$) in a laser with an increase in the pump current.

4.4 Gain Measurement using Unamplified Spontaneous Emission

Gain measurement using Hakki Paoli method has certain drawbacks. First of all the spontaneous emission profile from the facet of a laser represents only a portion of the whole spontaneous emission spectrum.¹ The gain calculation based upon facet emission becomes increasingly difficult as the current is raised to the threshold value, and beyond this point the spectral behavior of the gain in the laser cannot be deduced using the Hakki-Paoli method.¹ Besides this, as the precision of the gain measured is directly related to the magnitudes of the peaks and valleys of longitudinal mode spectra, a very high resolution spectra is needed for a precise determination of gain, which is a challenging task at low injection

levels. In addition, any inhomogeneities in the lateral profile of the mode over the laser facet can create complications while obtaining the data.¹¹ Another method of gain measurement which uses the unamplified spontaneous emission, first developed by Henry and Logau^{16,17}, offers solutions to these problems.

We will start by developing an expression relating gain in semiconductors with the spontaneous emission, an experimentally measurable entity. The experimental results obtained using this method for our lasers will then be presented and discussed.

4.4.1 Relationship between Absorption and Emission

Using equation 4.5 and 4.13 we may derive⁴

$$r_{sp}(h\omega) = \frac{4\bar{n}^2\alpha(h\omega) \int_{-\infty}^{\infty} D_c(E_1 + h\omega)f_c(E_1 + h\omega)D_v(E_1)(1 - f_v(E_1))dE_1}{h\lambda^2 \int_{-\infty}^{\infty} D_c(E_1 + h\omega)D_v(E_1)[f_v(E_1) - f_c(E_1 + h\omega)]dE_1} \quad (4.36)$$

and the substitution of the explicit expressions for quasi Fermi distributions, and rearranging the terms, leads us to the famous van Roosbroeck-Shockley relation

$$\alpha(h\omega) = \frac{r_{sp}(h\omega)h\lambda^2 \{ \exp(\frac{h\omega + E_{fv} - E_{fc}}{kT}) - 1 \}}{4\bar{n}^2} \quad (4.37)$$

which may then be rewritten as

$$\alpha(h\omega) = C_p \frac{S(h\omega)}{(h\omega)^2} \left[\exp\left(\frac{h\omega - \Delta E_f}{kT}\right) - 1 \right] \quad (4.38)$$

where $S(h\omega)$ is the spontaneous emission at photon energy $h\omega$ and ΔE_f is the quasi Fermi level separation given as $\Delta E_f = E_{fc} - E_{fv}$. C_p is a proportionality constant to be determined experimentally.

The above relation thus enables us to find gain $g(h\omega) = -\alpha(h\omega)$ by measuring the spontaneous emission^{8,32-34} provided we know the quasi Fermi level separation ΔE_f . The constant of proportionality C_p is determined by measuring

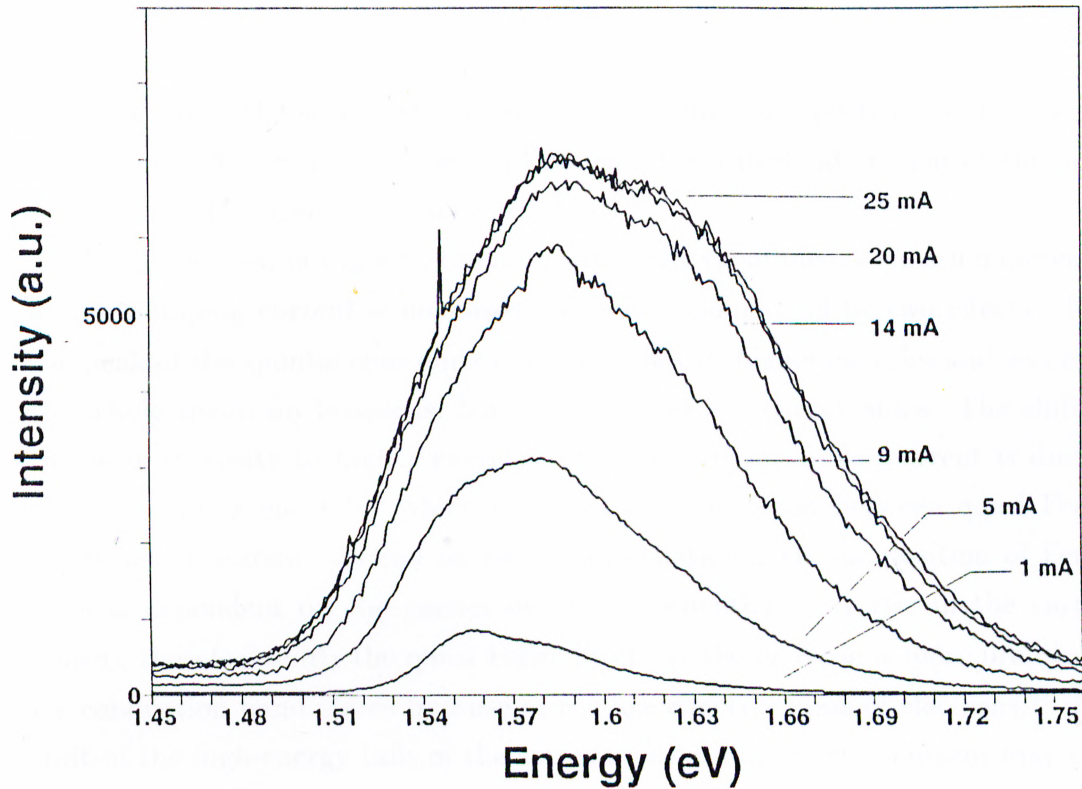


Figure 4.8: Unamplified Spontaneous Emission Spectra
Spontaneous emission from the top of the ridge in ITO-contact Lasers at different currents.

spontaneous emission at threshold value and then scaling gain, obtained from this data, to the known threshold value

$$g_{th} = \frac{1}{\Gamma} \left(\alpha_i + \frac{1}{L} \ln\left(\frac{1}{R}\right) \right) \quad (4.39)$$

All other gain values may then be scaled using C_p .

4.4.2 Gain vs. Injection Current

To measure gain using this method a set of spontaneous emission spectra, for different pumping current levels, was obtained from the ridge of our GRIN SCH lasers. The optical setup to obtain the data was similar to the one used for Hakki-Paoli method. The only difference was that the laser was placed in such a way that instead of the facet, now the ridge of the laser was imaged on the

entrance slit of the spectrometer. Spontaneous emission spectrum at 1, 5, 9, 14, 20 and 25 mA current levels were obtained. The threshold current of the laser was 20 mA. The spectra are shown in Fig.4.8.

As can be seen in Fig.4.8, the intensity of the spontaneous emission increases as the pumping current is increased. This is accompanied by two effects; first the peak of the spontaneous emission shifts towards higher energies and secondly the whole spectrum broadens, both at high and low energy sides. The shift of the peak intensity to higher energies with an increase in the current is due to the band filling effect^{31,30} which increases the separation between quasi Fermi levels of the system. As can be seen from equation 4.41, the position of Fermi level is dependent on the carrier density exponentially. A rise in the carrier density therefore shifts the quasi Fermi level but the increase is more prominent for conduction band states because of the low effective mass of electrons.²⁴ The shift of the high-energy tails of the spectra with an increase in current may also be explained by similar reasoning; as the band filling starts the higher energy transitions become apparent. At low injection current the transition from the conduction band to heavy and light hole states in the valence band can easily be distinguished but at higher injection levels these fine features are lost due to spectral broadening.

The shift of the low energy tail though is due to shrinkage in the band gap caused by band gap renormalization.^{39,37,38} The band gap renormalization effect is due to many-body interactions at high carrier densities. It can be seen that the band gap renormalization causes a much weaker shift than band filling. It is also worth noting that at around 20 mA, the spontaneous emission spectra from the ridge spans an energy range of approximately 300 meV, a much wider range than obtained by Hakki-Paoli method.

We see a sharp peak at around 1.54 eV, for 20 and 25 mA spectra. This is the leakage of the laser emission due to scattering in the waveguide or from collection optics. A similar effect was observed by Hirayama et. al.⁴⁵ where the lasing peak lied at a lower energy than the spontaneous emission peak. This lasing peak may serve the purpose of a reference point and is left intentionally in subsequent

calculation of gain.

To calculate the quasi Fermi level separation we first estimated the injected carrier density using the relation^{4,2}

$$n = \frac{j\tau_s}{qa_x} \quad (4.10)$$

where j is the injected current density, τ_s is the recombination lifetime, q is the carrier charge and d is the thickness of the recombination region, thickness of the quantum well in our case. The value of τ_s was taken to be 0.5 ns.⁴⁴ The carrier densities for the range of pumping current used in our experiment, were on the order of 10^{18}cm^{-3} .

The quasi Fermi levels were then calculated using the equation

$$E_{f,c,v} = E_{c,v} \pm kT \ln \left\{ \exp \left[\frac{n\pi a_x \hbar^2}{m_e kT} \right] - 1 \right\} \quad (4.11)$$

and the spontaneous emission curves were then converted to gain using the van Roosbroeck-Shockley relation. The results are shown in Fig.4.9.

The gain curves for 1 and 5 mA current levels show absorption at all wavelengths. At these current levels the carrier density is insufficient to cause a quasi Fermi level separation greater than the 1.54 eV limit, the energy difference between the first conduction subband electron state and the first valence subband heavy hole state. The amplification starts at higher currents. The general features of the gain curves, with the exception of the sharp drop at the higher energy side of the curves, are similar to the spontaneous emission curves. This is to be expected due to the van Roosbroeck-Shockley relation according to which the gain is directly proportional to the spontaneous emission.

Another feature of the gain curves is the saturation of gain beyond the threshold point. The pinning of spontaneous emission is also obvious from the spontaneous emission spectra. This pinning behavior is then reflected in the gain curves. The gain saturation effect has been examined previously by several investigators.^{9,42,41} The process of gain saturation may be explained as follows.

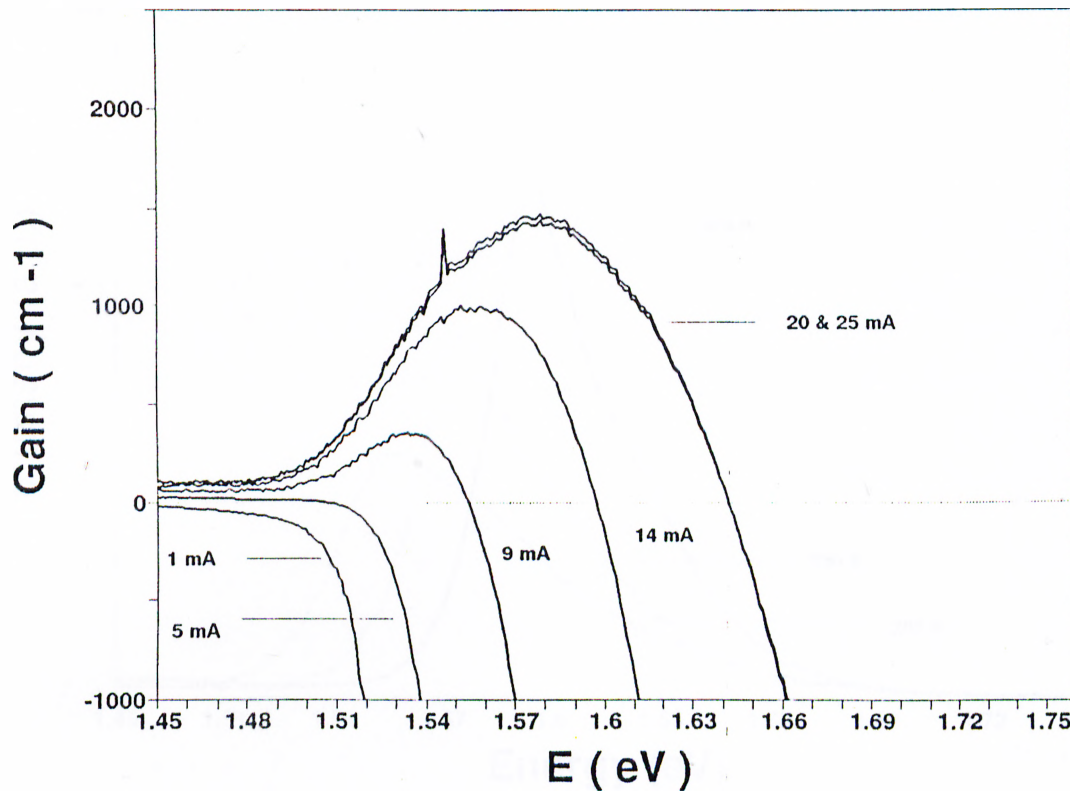


Figure 4.9: Measured Gain in Laser

Material gain measured using unamplified spontaneous emission from the top of the ridge in ITO-contact Lasers

An excited semiconductor crystal amplifies radiation if it satisfies the Bernard-Duraffourg condition. However, the radiation intensity in the resonator cannot increase without limits, since at high photon densities the carrier concentration in the conduction and valence bands decreases markedly. This in turn causes the Fermi-level to shift so that quasi-Fermi level separation decreases and so does the number of states that satisfy Bernard-Duraffourg condition.

Measurement of gain using USE method requires a knowledge of quasi-Fermi level separation and internal losses. Different techniques have been employed so far by several researchers^{8,20,24,30} to obtain these parameteres and as yet no consensus exists on how to deduce the values of these parameters most precisely.

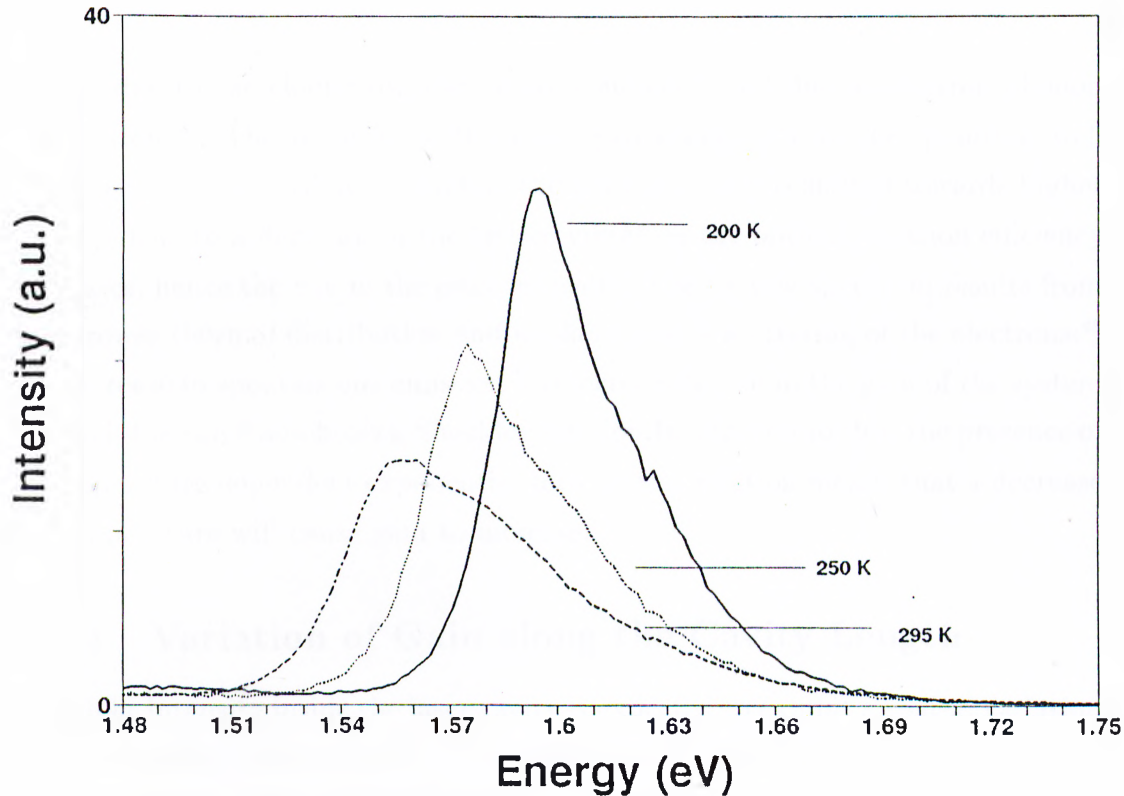


Figure 4.10: Unamplified Spontaneous Emission vs Temperature
The changes in Unamplified Spontaneous Emission with a decrease in temperature

4.4.3 Effect of Temperature on Gain

Gain in semiconductors is temperature dependent.⁴⁹ The effect of temperature on our GRINSEL lasers was investigated by measuring the spontaneous emission at three different temperatures. The laser was placed in a cryostat and the spontaneous emission from the ridge was collected at temperatures of 295 , 250 and 200 K. At each temperature the spontaneous emission was measured for a set of various injection levels. The results are shown in Fig.4.10 .

Three effects deserve comment ; First, as the temperature is decreased we observe that the peaks of the curves shift towards higher energy; second, the peak intensity increases and finally the whole curve becomes narrower. A qualitative explanation of these effects can be given as follows. The decrease in temperature is accompanied by an increase of the band gap. The change in band gap energy

occurs due to the changes in the lattice constant⁵¹ and due to electron phonon interaction.⁵¹ The increase in the band gap energy effects the quantum well subband states as well and therefore the peak intensity is shifted towards higher energy. Due to a decrease in the lattice vibration the optical emission efficiency increases, hence the rise in the peak intensity. The narrow spectrum results from a narrower thermal distribution and weaker phonon scattering of the electrons.⁴⁹

Increase in spontaneous emission is directly reflected in the gain of the system through the van Rosebroeck-Shockley relation. In addition to this, the presence of a temperature dependent exponential term in this relation means that a decrease in temperature will cause gain to increase.

4.4.4 Variation of Gain along the Cavity Length

The light intensity inside the laser cavity is expected to exhibit a spatial variation along the length of the cavity.^{46,47,43} A light wave travelling along the cavity axis is modulated by the spatially varying absorption coefficient inside the cavity and by the losses faced at the mirror ends. Due to the current dependence of absorption coefficient, the spatial profile of the light is also dependent on the injected carrier density. As the active medium of the cavity makes a transition from the loss to gain, the light profile also exhibits changes. Phillips et al⁴⁶ have stated that the spontaneous emission emitted perpendicular to the laser axis gives an accurate indication of the relative carrier density because it is not modified by the gain or absorption in the active layer.

The spatial distribution of spontaneous emission from the ridge of our GRINSEL laser along the cavity axis and measured at very low injection, i.e. 0.6 mA, is shown in Fig.4.11. Emission from about a $10\mu\text{m}$ portion of the ridge was collected each time and steps of $50\mu\text{m}$ were taken between two consecutive data collection points. The profile shows a sharp drop in the spontaneous emission intensity near the mirror ends of the cavity. The intensity rises towards the middle and reaches its maximum at around the center of the cavity. This is understandable because at this low injection level the medium is absorbing

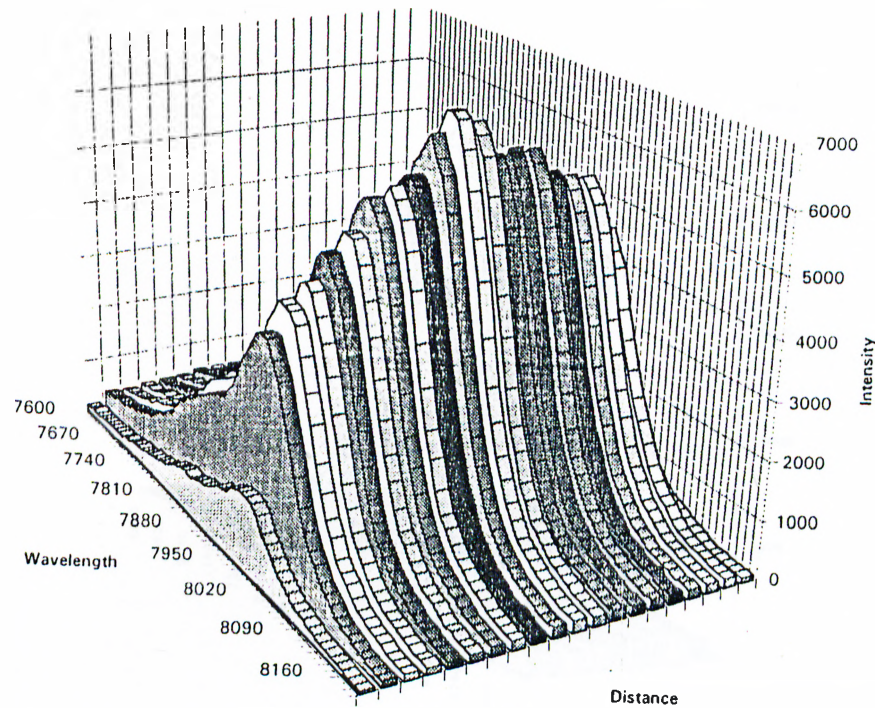


Figure 4.11: Spontaneous Emission along Cavity Length at Very Low Injection
The change in Spontaneous Emission along the length of the laser cavity at 0.6 mA

at all wavelengths. The spontaneous emission therefore represents a localized contribution of generated light because any photons attempting to travel inside the cavity get absorbed before they go far. The losses at the mirror ends, due to non radiative surface recombination and mirror emission, cause a drop in the spontaneous emission.

This trend changes as the current is increased to 6 mA. As shown in Fig.4.12. The difference between the edge and the center now decreases. The overall injected carrier density increases and the absorption coefficient decreases. The spatial behaviour of light is therefore modified because the light can travel a longer distance in the cavity before getting absorbed. Though the overall intensity of spontaneous emission increases, the difference between the emission from the facet side and the center now decreases.

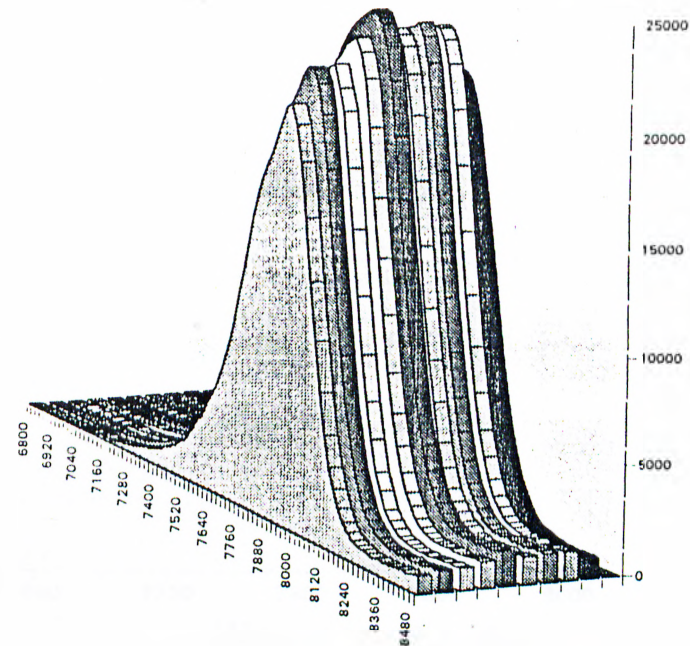


Figure 4.12: Spontaneous Emission along Cavity Length at 6 mA
The change in Spontaneous Emission along the length of the laser cavity at 6 mA.

The situation is not so simple when the active layer becomes amplifying. As the stimulated emission becomes dominant, an estimate of photon and carrier densities inside the cavity requires solution of the rate equations describing the behaviour of electrons in semiconductors in the presence of an electromagnetic field.⁴³ It has been shown, however, that above threshold the gain at the center of the cavity is higher than at the ends. The difference though is quite small and is difficult to observe unless very high injection currents are used or the mirror reflectivities are decreased. The data taken from a laser at 35 mA, where the threshold current of the laser is 20 mA, is shown in Fig.4.13. The curves are from the edge and the center of the cavity but do not show any remarkable difference.

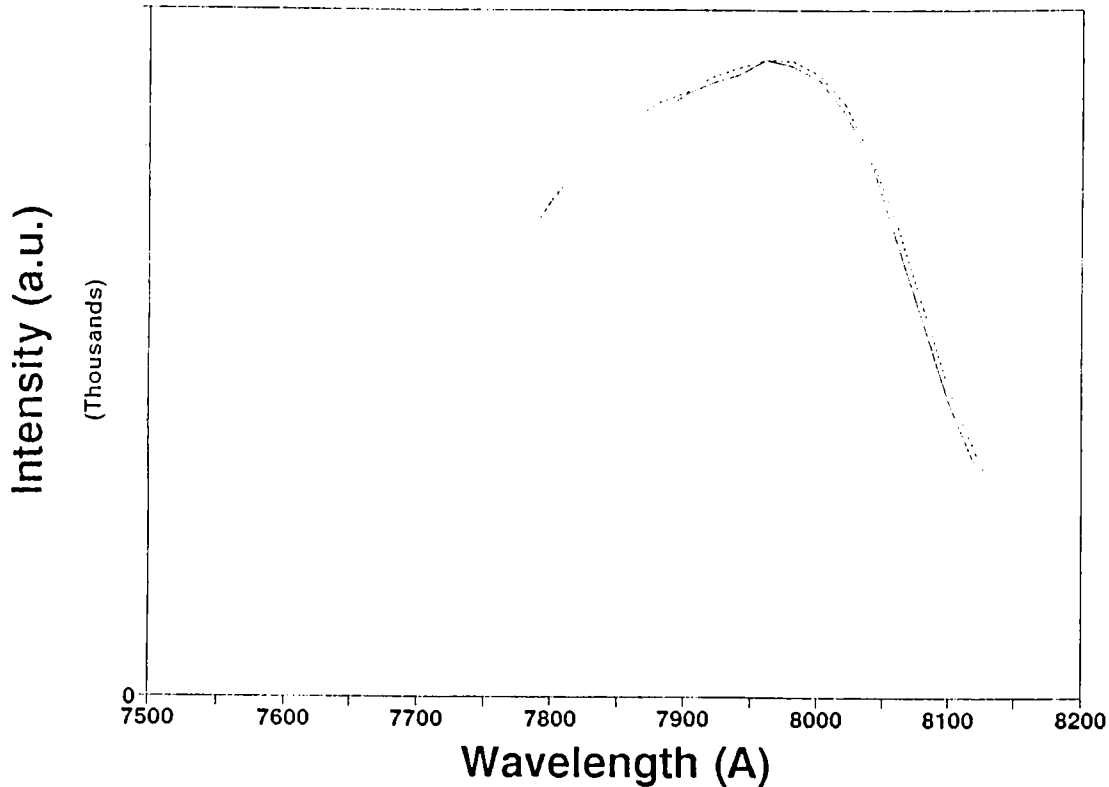


Figure 4.13: Spontaneous Emission along Cavity Length above Threshold. The Spontaneous Emission from the edge (dotted line) and the center (solid line) of the cavity at current above threshold.

4.4.5 Lateral variation in Spontaneous Emission Profile

So far we have discussed the unamplified spontaneous emission emerging from the ridge of the laser through the transparent ITO contacts. However, light is also emitted from a region outside the ridge of the laser. The oxide layer underneath the ITO p-type contact is transparent to the light generated in the quantum well and hence the p-type ITO contact allows us to analyze the light being emitted from an off ridge region. Therefore, beside the longitudinal spatial variation in the emission we may analyze the lateral spatial changes in the spontaneous emission too.

The light collected from the off ridge area is a combination of two different type of signals. First is the light emitted in the active layer of the ridge and travelling in the lateral direction. During its travel this light gets reabsorbed in

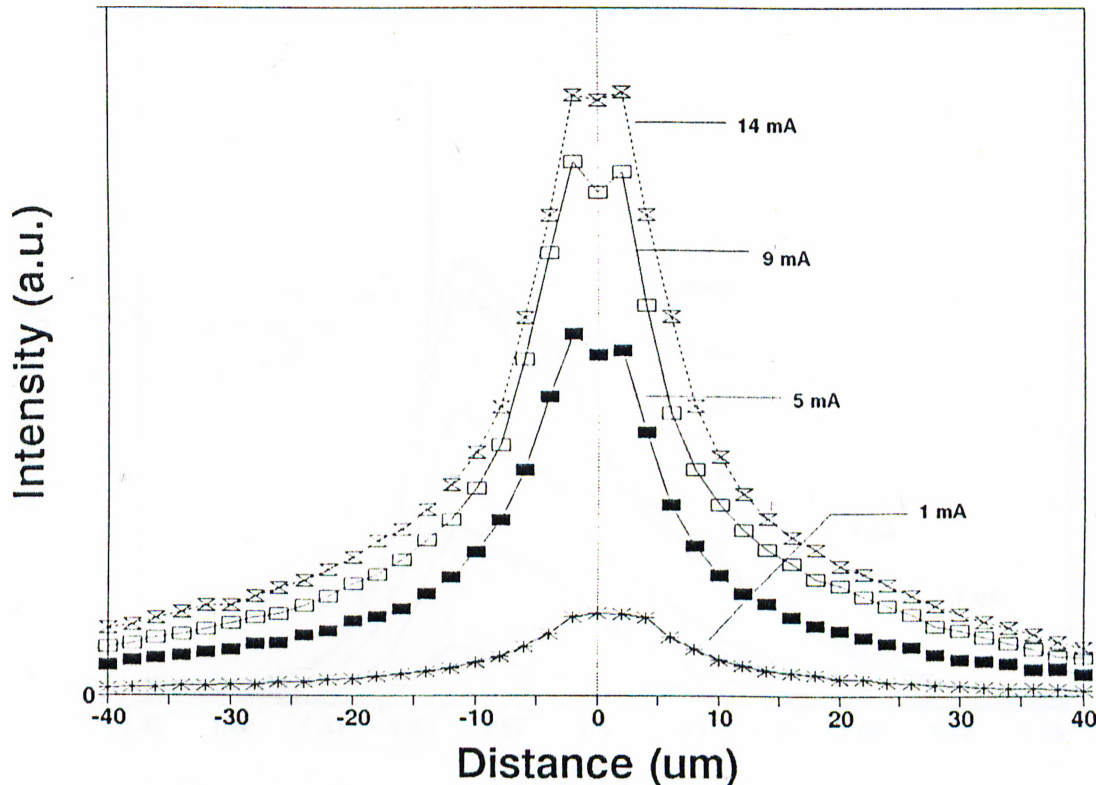


Figure 4.14: Lateral Profile of Spontaneous Emission Intensity

The lateral distribution of the peak spontaneous emission intensity at different currents. Distances are measured from the ridge.

the unpumped quantum well layer and reemits, and therefore the intensity of this light gradually decreases. The second contribution comes from the laterally diffusing injected carriers which could not be confined to the ridge area under injection and recombine at a distance from the ridge. The current due to these carriers is termed as the leakage current.⁴⁸ These two contributions produce an interesting emission spectra.

A set of spontaneous emission spectra collected from $20\mu m$ off the ridge area at different current levels is shown in Fig.4.15. The sharp peak in the 20 mA current spectra is the lasing peak scattered from the optics. The most important difference between this off ridge emission spectra and the one from the ridge area is that at higher current densities the peak intensity position does not shift and the broadening of the spectra is much lower. The features of the heavy hole

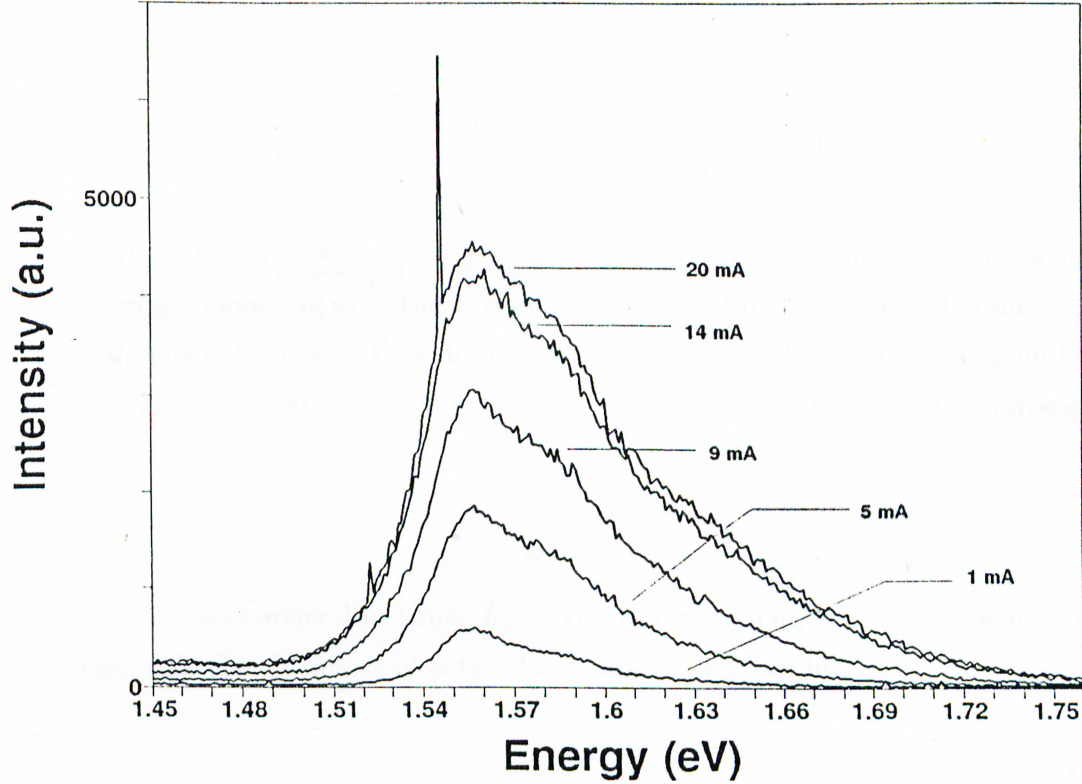


Figure 4.15: Spontaneous Emission from Off-Ridge Area

The development of spontaneous emission spectrum intensity with injection current from 20 μm off-ridge area.

transitions and light hole transitions are also evident at higher currents.

The lateral profile of the peak intensity of the spontaneous emission was measured for our GRINSEL laser for a set of different currents and is shown in Fig.4.14 . This profile indicates the extent of the lateral penetration of leakage current. It was shown by Casey and Panish² that the lateral distribution of the carrier density may be modeled using the equation

$$n(x) = n_1 + \left(\frac{1}{l_o + L_n}\right) \left(\frac{I_o \tau_n}{qLd}\right) \cosh\left(\frac{x}{L_n}\right) \exp\left(\frac{-S}{2L_n}\right) \quad (4.42)$$

where $n_1 = \left(\frac{I_r \tau_n}{qSLd}\right) \left[1 - \cosh\left(\frac{x}{L_n}\right) \exp\left(\frac{-S}{2L_n}\right)\right]$, for the carriers inside the ridge area and

$$n(x) = C \exp\left[\frac{-(|x| - \frac{S}{2})}{L_n}\right] + l_o \left(\frac{1}{l_o^2 - L_n^2}\right) \left(\frac{l_o \tau_n}{qLd}\right) \exp\left[\frac{-(|x| - \frac{S}{2})}{l_o}\right] \quad (4.43)$$

where $C = \left[\frac{\frac{l_o \tau_n}{qS L d}}{1 + \coth\left(\frac{S}{2L_n}\right)} - \left(\frac{1}{l_o^2 - L_n^2}\right) \left(\frac{l_o \tau_n}{qLd}\right) \left(\frac{l_o + L_n \coth\left(\frac{S}{2L_n}\right)}{1 + \coth\left(\frac{S}{2L_n}\right)}\right)\right]$, for the carriers outside the ridge region. $n(x)$ is the carrier density as a function of the distance x . The total injected current I_t is divided into two parts ; I_r is the current under the ridge and I_o is the leakage current flowing in $\pm x$ direction, related through the equation

$$I_t = I_r + 2I_o \quad (4.44)$$

τ_n is the carrier life time, L_n is the diffusion length, S is the width of the ridge, d is the thickness of active layer, and l_o is given by

$$l_o = \frac{2L}{\beta \rho_s I_o} \quad (4.45)$$

L is the cavity length and ρ_s is the resistivity. β is the exponential junction parameter q/nkT .

Using this model we have estimated the carrier concentration corresponding to the lateral variation of spontaneous emission. This carrier density is strongly dependent on various parameters such as diffusion coefficient of carriers, carrier lifetime, resistivity etc. We find that the peak carrier concentration is on the order of a few times 10^{18}cm^{-3} , which is in accordance with previous results.⁴

Chapter 5

Conclusions

The aim of this work was to analyze the behavior of gain as a function of some operational parameters in quantum well semiconductor lasers.

In this study we fabricated GRINSCII single quantum well ridge lasers. Two different type of lasers were fabricated. For the first type of laser we made a $7 \mu\text{m}$ opening in the $50 \mu\text{m}$ ridge, in the top p-type metal alloy ohmic contacts, which allows collection of light both from the facet as well as from the plane perpendicular to the facet. However during our attempts to fabricate narrower ridge lasers operating in a single mode, so that they can be used in measurement of gain from both the facet emission (Hakki- Paoli method) and the window emission, certain problems were faced in the optimization of the fabrication process. We therefore developed a new laser structure to overcome these problems. The second type of lasers used transparent ITO contacts and lasers with $4 \mu\text{m}$ ridge were fabricated. The fabrication process of both these types of lasers were analyzed. The threshold current of the second type of lasers were lower due to narrower ridges and subsequent measurements of gain were made on these type of lasers. Another advantage offered by the ITO contact lasers was that the collection of spontaneous emission could be made not only from the ridge itself but from the surrounding areas as well.

These lasers were then characterized and the electrical and optical characteristics of the lasers were investigated. The threshold currents as low as 14 mA

were found for ITO contact lasers. The quantum differential efficiencies reaching upto 60 % were found in some lasers. The series resistance of the lasers were in the range of 50 to 100 ohms.

Gain in these lasers was then measured using two different techniques. First method, called the Hakki-Paoli method, used facet emission of the laser to obtain gain in the lasers. The longitudinal mode spectra of the lasers were obtained for different currents and these spectra were then converted to the gain spectra. From the spectral behavior of gain the internal losses of the laser were estimated to be about 7 cm^{-1} . We found that the spectral broadening of gain increases as current is increased to its threshold value. The red shift of the spectral edge is attributed to the bandgap renormalization effects while the blue shift of the spectral edge is explained in terms of band filling effects. Measurement of spectral distribution of gain above threshold becomes impossible as the laser starts to lase, drastically narrowing the spectral bandwidth of the emitted light. We also note that uncertainties in the measurement of gain increase at the spectral edges as modulation depths become comparable to noise, and become especially acute at low injection currents. While this can be improved with larger data accumulation times, large spectral bandwidths over which data must be collected with maximum resolution makes it not feasible beyond reasonable time periods. Some of the shortcomings of the HP method, such as inability to measure gain above threshold, are overcome by unamplified spontaneous emission method. In this method light emitted in a direction perpendicular to the quantum well plane, was measured. Using the van Roosbroeck-Shockley expression, relating spontaneous emission to gain in lasers, these spectra were transformed to reveal the gain in these lasers. Material gain values as high as 1500 cm^{-1} were obtained for these lasers. This is about an order of magnitude greater than gain in bulk semiconductors.

Calculation of gain from USE data requires a precise knowledge of the quasi-Fermi level separation. Several authors⁸ have estimated this value by subtracting the voltage drop due to series resistance from the bias voltage. In the case of ITO contact lasers this introduces large errors into the calculation since the

voltage drop across the junction is considerably smaller than the drop on the series resistance of the diodes. We therefore calculated the quasi-Fermi level separation by estimating the injected carrier density from the injected current density. As our data on the lateral profile of the spontaneous emission shows, there is considerable leakage current present in these diodes even though the mesa was etched quite deep. Our calculation of the carrier density does not take into account this leakage current and therefore over estimates both the injected carrier density and the quasi-Fermi level separation. This then leads to an overestimation of the gain. Saturation of gain beyond threshold may provide a reference point that may limit the magnitude of the overestimate if a precise determination of the lasing threshold is made. Due to the difficulty in defining a precise threshold and limited data we suspect that the gain at saturation in Fig. 4.9 is an over estimate that leads to lasing below maximum gain.

The gain spectra obtained using the USE method also showed broadening as the injection current of the lasers was increased. The peak gain shifted towards higher energies and its value increased and a broadening of the whole gain spectrum, at both the low and high energy side of the spectrum, was observed. These effects were again attributed to the bandfilling and the band gap renormalization effect in the quantum well. We were also able to measure gain at and above the threshold current using this method. As expected, a saturation of the gain was observed after the threshold current of the laser was reached.

The effect of temperature on the gain was also investigated. It was observed that gain in lasers increased with a decrease in the temperature. This was accompanied by a shift of the peak gain towards higher energies and a narrowing of the whole gain spectra. The blue shift of the gain is understood in terms of the temperature dependence of band gap. Other effects are due to reduced carrier-phonon scattering as well as temperature dependence of the quasi Fermi levels.

It was also observed that the distribution of gain in the lasers along the cavity direction is not uniform. The spontaneous emission from an area near the mirror

ends of the cavity was lower than the emission from the middle.

Lateral spontaneous emission profile shows that there is some leakage of current in the lateral direction lowering the differential efficiency of the lasers. Using a simple model for carrier diffusion along the leakage direction it is possible to obtain the carrier density profile during injection, using the lateral profile of the spontaneous emission. Such a model, however, is very sensitively dependent on the parameters such as diffusion coefficient and diffusion length, carrier lifetime in various layers, resistivity etc. and care should be taken to obtain reliable data.

In conclusion we may say that several aspects of the gain in the quantum well lasers were successfully investigated in this study and results obtained by us are satisfactorily in accordance with the results obtained by other researchers previously. Many features of gain in semiconductor laser diodes, however, remain to be resolved. Measurement of gain in new laser material systems, especially in the 1.3 -1.55 μm range, suitable for Fiber Optical communication systems is important. Similarly, gain in material systems lasing in blue, still needs to be investigated. Gain calculations need also be tested for the extreme limits of laser diodes design parameters, such as, long cavities, large and very narrow mesa widths etc.

Bibliography

- [1] G. H. B. Thompson, *Physics of Semiconductor Laser Devices*, Avon: John Wiley & Sons, (1980).
- [2] H. C. Casey, and M. B. Panish, *Hetrostructure Lasers*. New York: Academic, (1978).
- [3] R. Dingle, W. Wiegmann, and C. H. Henry, Quantized states of confined carriers in very thin AlGaAs-GaAs hetrostructures, *Phys. Rev. Lett.* , **33**:827, (1974).
- [4] K. J. Ebeling, *Integrated Opto-Electronics*, Berlin: Springer-Verlag, (1993).
- [5] J. P. van der Ziel, R. Dingle, R. C. Miller, W. Wiegmann, and W. A. Nordland, Laser oscillation from quantum states in very thin GaAs-AlGaAs multilayer structure, *Appl. Phys. Lett.* , **26**:463, (1975).
- [6] W. T. Tsang, Extremely low threshold AlGaAs graded index waveguide separate confinement hetrostructure lasers grown by molecular beam epitaxy, *Appl. Phys. Lett.* , **40**:217, (1982).
- [7] P. Rees, and P. Blood, Derivation of gain spectra of laser diodes from spontaneous emission measurements, *IEEE J. Quantum Electron.* , **QE-31**:1047, (1995).
- [8] M. P. Kesler, and C. Harder, Excitonic Effects in gain and index in AlGaAs quantum well lasers, *Appl. Phys. Lett.* **57**:123, (1990).

- [9] B. Mroziewicz, M. Bugajski, and W. Nakwaski, *Physics of Semiconductor Lasers*, Amsterdam: Nort Holland, Inc. , (1991).
- [10] R. M. Warner, and B. L. Grung, *Semiconductor Device Electronics*, Holt, Reinhart and Winston, Inc. , (1991).
- [11] Y. Suematsu, and A. R. Adams, *Semiconductor Lasers and Photonic Integrated Circuits*, London: Chapman & Hall, (1994).
- [12] R. L. Liboff, *Introductory Quantum Mechanics*, Addison-Wesley publishing Co. , (1980).
- [13] B. W. Hakki, and T. L. Paoli, Gain spectra in GaAs double hetrostructure injection lasers, *J. Appl. Phys.* , **46**:1299, (1975).
- [14] B. W. Hakki, Carrier and gain spatial profiles in GaAs stripe geometry lasers, *J. Appl. Phys.* , **44**:5021, (1973).
- [15] B. W. Hakki, and T. L. Paoli, CW degradation at room temperature of GaAs double hetrostructure junction lasers. II. Electronic gain, *J. Appl. Phys.* , **44**:4113, (1973).
- [16] C. H. Henry, R. A. Logan, and F. R. Merritt, Measurement of gain and absorption spectra in AlGaAs buried hetrostructure, *J. Appl. Phys.* **51**:3042, (1980).
- [17] C. H. Henry, Theory of the linewidth of semiconductor lasers, *IEEE J. Quantum Electron.* , **QE-18**:259, (1982).
- [18] C. H. Henry, R. A. Logan, and K. A. Bertness, Spectral dependence of the change in refractive index due to carrier injection, *J. Appl. Phys.* **52**:4457, (1981).
- [19] R. H. Yan, S. W. Corzine, L. A. Coldren, and I. Suemune, Corrections to the expressions for gain in GaAs, *IEEE J. Quantum Electron.* , **QE-26**:213, (1990).

- [20] P. Blood, S. Colak, and A. I. Kucharska, Influence of broadening and high-injection effects on GaAs-AlGaAs quantum well laser, *IEEE J. Quantum Electron.* , **QE-24**:1593, (1988).
- [21] M. Osinski, and J. Buus, Linewidth broadening factor in semiconductor lasers- An overview, *IEEE J. Quantum Electron.* , **QE-23**:9, (1987).
- [22] M. P. Kesler, and E. P. Ippen, Subpicosecond gain dynamics in AlGaAs laser diodes, *Appl. Phys. Lett.* , **51**:1765, (1987).
- [23] W. H. Knox, D. S. Chemla, G. Livescu, and J. E. Henry, Femtosecond Carrier thermalization in dense Fermi seas, *Phys. Rev. Lett.* **61**:1290, (1988).
- [24] P. S. Zory, *Quantum Well Lasers*, San Diego: Academic Press, Inc. , (1993).
- [25] M. Asada, A. Kameyama, and Y. Suematsu, Gain and intervalence band absorption in quantum-well lasers, *IEEE J. Quantum Electron.* , **QE-20**:745, (1984).
- [26] D. Ahn, Collision broadening of optical gain in semiconductor lasers, *J. Appl. Phys.* **65**:4517, (1989).
- [27] M. Yamanishi, and Y. Lee, Phase dampings of optical dipole moments and gain spectra in semiconductor lasers, *IEEE J. Quantum Electron.* , **QE-23**:367, (1987).
- [28] M. Yamanishi, and I. Suemune, Comment on polarization dependent momentum matrix elements in quantum well lasers, *Japan J. Appl. Phys.* **23**:L35, (1984).
- [29] M. Asada, Intraband relaxation time in quantum well lasers, *IEEE J. Quantum Electron.* , **QE-25**:2019, (1989).
- [30] E. A. Avrutin, I. E. Chebunina, I. A. Eliachevitch, S. A. Gurevich, M. E. Portnol, and G. E. Shtengel, TE and TM optical gains in AlGaAs/GaAs single quantum well lasers, *Semicond. Sci. Technol.* , **8**:80, (1993).

- [31] G. Hunziker, W. Knop, and C. Harder, gain measurements on one, two and three strained GaInP quantum well laser diodes, IEEE Trans. Quantum Electron. , **QE-30**:2235, (1994).
- [32] M. P. Kesler, and C. Harder, Spontaneous emission and gain in AlGaAs quantum well lasers, IEEE J. Quantum Electron. , **QE-27**:1812, (1991).
- [33] M. P. Kesler, C. Harder, and E. E. Latta, Carrier heating in AlGaAs single quantum well laser diodes, Appl. Phys. Lett. , **59**:2775, (1991).
- [34] C. Harder, P. Buchmann, and H. Meier, High power ridge-waveguide AlGaAs GRINSCHE laser diode, Electron. Lett , **22**:1081, (1986).
- [35] C. H. Chinn, P. S. Zory, and A. R. Reisinger, A model for GRINSCHE SQW laser diodes, IEEE J. Quantum Electron. , **QE-24**:2191, (1988).
- [36] Y. Arakawa, and A. Yariv, Theory of gain, modulation response and spectral linewidth in AlGaAs quantum well lasers, IEEE J. Quantum Electron. , **QE-21**:1666, (1985).
- [37] C. Ell, H. Haug, and S. W. Koch, Many body effects in gain and refractive index spectra of bulk and quantum well semiconductor lasers, Opt. Lett. **14**:356, (1989).
- [38] S. Tarucha, H. Kobayashi, and H. Okamoto, Carrier induced energy gap shrinkage in current injection GaAs/AlGaAs MQW heterostructure, Japan J. Appl. Phys. **23**:874, (1984).
- [39] D. A. Kleinman, and R. C. Miller, Band gap renormalization in semiconductor quantum well containing carriers, Phys. Rev. B, **32**:2266, (1985).
- [40] A. Tomita, and A. Suzuki, Carrier induced lasing wavelength shift for quantum well laser diodes, IEEE J. Quantum Electron. , **QE-23**:1155, (1987).

- [11] J. Butty, G. Bongiovanni, and J. L. Staehli, Optical amplification and its saturation in semiconductor quantum wells, *Journal De Physique*, **3**:31, (1993).
- [12] S. L. Chuang, J. O’Gorman, and A. F. J. Levi, Amplified spontaneous emission and carrier pinning in laser diodes, *IEEE J. Quantum Electron.*, **QE-29**:1631, (1993).
- [13] S. Hasuo, and T. Ohmi, Spatial distribution of light intensity in the Injection lasers, *Jap. J. Appl. Phys.*, **13**:1429, (1974).
- [14] Z. M. Wang, J. Windscheif, D. J. As, and W. Jantz, High resolution carrier temperature and lifetime topography of semi-insulating GaAs using spatially and spectrally resolved photoluminescence, *J. Appl. Phys.*, **73**:1430, (1993).
- [15] H. Hirayama, J. Yoshida, Y. Miyake, and M. Asada, Estimation of carrier capture time of quantum well lasers by spontaneous emission, *Appl. Phys. Lett.*, **61**:2398, (1992).
- [16] M. R. Phillips, T. E. Darcie, and E. J. Flynn, Experimental measure of dynamic spatial hole burning in DFB lasers, *IEEE Photonics Tech. Lett.*, **4**:1201, (1992).
- [17] R. Schatz, Longitudinal spatial instability in symmetric semiconductor lasers due to spatial hole burning, *IEEE J. Quantum Electron.*, **QE-28**:1443, (1992).
- [18] S. Y. Hu, D. B. Young, A. C. Gossard, and L. A. Coldren, The effect of lateral leakage current on the experimental gain-current density curve in quantum well ridge waveguide lasers, *IEEE J. Quantum Electron.*, **QE-30**:2245, (1994).
- [19] L. D. Zhu, B. Z. Zheng, and G. A. B. Feak, Temperature dependence of optical gain, quantum efficiency, and threshold current in GaAs/AlGaAs

graded index separate confinement heterostructure single quantum well lasers, IEEE J. Quantum Electron. , **QE-25**:2007, (1989).

[50] J. T. Verdeyen, Laser Electronics, New Jersey: Prentice Hall, (1995).

[51] Sadao Adachi, GaAs and related materials, World Scientific publishing Co. , (1994).